Universitetet i Stavanger

FACULTY OF SCIENCE AND TECHNOLOGY

MASTER'S THESIS

Study program/specialization: Petroleum engineering Drilling and well engineering	Spring semester 2021 Open access
Author: **Milad Rezaei**	_____ (Author's signature)

Faculty Supervisor:
Dr. Mahmoud Khalifeh
Dr. Arild Saasen
External supervisors: Bodil Aase

Title of master's thesis:
Barite Sag Settling measurement techniques – direct method

Credits: 30 ECTS

Keywords: Settlement Barite Sag measurement Direct method Indirect method Buoyancy effect	Number of pages: 61

Acknowledgement

I would first like to thank Dr. Mahmoud Khalifeh, my thesis supervisor at the University of Stavanger. The door of his office was always open whenever I ran into a trouble spot or had a question about my research. He consistently allowed this work to be my own but steered me in the right direction whenever he thought I need it. I would also like to thank Prof. Arild Saasen for exciting discussions and valuable references for my work

I would also like to thank Bodil Aase, my external supervisor from Equinor, to assign me an interesting theme for my thesis and arrange a collaboration between the University of Stavanger and Equinor.

I would like to thank uis for welcoming me and allowing me to perform all needed experiments at their laboratories.

Further, I would like to big thank Jostein Djuve and Kim Andre Nesse Vorland for their support throughout the work done in the laboratories at the University of Stavanger.

At last, I would like to thank Tor Henry, Lorents, and Kjell Morten from equinor and Marco Marien from Inphase for making me motivated and their help, support, and good discussions throughout the work.

Abstract

One of the main roles of drilling fluid is controlling the downhole pressure. Weighting materials are employed in drilling fluid for this aim. Barite is the most common agent, which is used for increasing density. There are some factors, such as gravitational force, damage, or degradation of polymers which cause a sluggish phenomenon called barite sag. During the barite sagging, suspended particles start to settle and separate from the liquid phase, and the fluid column gets denser at the bottom and less on top. Barite can settle out from drilling fluid during tripping in and tripping out when circulation is stopped. Meanwhile, dynamic barite sag can occur during circulation. Particle settlement can be measured by two different methods, including direct and indirect measurements. In the direct method, measurement is based on sag and fluid density weight, while the indirect evaluates the particle settling by transit time. Direct measurement is one of the methods, which has not been investigated experimentally while there are indirect methods using ultra-sonic employed to measure the barite settlement. In this work, barite particle settlement was inquired by direct measurement and then correlated with indirect results. In a basic system, direct measurement has been done by sedimentation rate criteria. Mechanical properties analyser was used to record the time taken to transfer the compressional wave from transducer to receiver through the vessel, which is filled by fluid sample. Several tests calibrated the systems regarding reference samples that had different xanthan gum content with constant barite. Then, the severity of barite sag was investigated by water-based and oil-based fluid after hot rolling in a modified system. Based on the measurements and results, empirical correlations for reference sample and real sample have been proposed to analyse the fluid behavior.

Results from the tests clearly demonstrated that the sedimentation rate increased dramatically in the first phase of sagging and then continued gradually. In the first test running, a large number of suspended particles started to settle in the MPro vessel. Compressional waves stroked the particles and made vibrations. This vibration took a long time to travel the wave from the transducer to the receiver. During the settlement, the waves were transferred in shorter transit time due to the less suspended particles, and then transit time decreased.

List of Contents

Abstract iii

List of Contents iv

List of Figures vi

List of Tables viii

1. Introduction 1

1.1 objectives 1

2. Literature Review and Background Theory 2

2.1 The Effect of particle settlement barite on completion and drilling fluid 2

2.2 Basics of settlement 4

2.3 Barite sag 5

2.4 Mechanisms of barite settlement 6

2.4.1 Static condition (Boycott and Hindered effect) 6

2.4.2 Dynamic condition 9

2.4.3 The effects of particle properties and fluid rheology on settlement 9

2.5 Barite sag measurement techniques 16

2.5.1 Static sag testing 17

2.5.2 Viscometer sag testing 18

2.5.3 Sag flow loop test 19

2.5.4 High angle sag test 21

2.5.5 ultrasonic measurement 21

2.5.6 Sag detection by nuclear magnetic resonance 22

3. Methodology and Experimental work 23

3.1 Equipment 23

3.1.1 Transparent pipe 23

3.1.2 Adventurer Balances (Lab Scale) 24

3.1.3 Mechanical Properties Analyzer (MPRO) 24

3.1.4 Hei-TORQUE 400 (Mixer) 25
3.1.5 Hot roller (oven) 26
3.1.6 Rotational Viscometer 27
3.2 Mix designs 28
3.2.1 reference samples 28
3.2.2 Real samples 29
3.3 Experimental Methods 30
3.3.1 Drilling fluid preparing and mixing procedure: 30
3.4 Test procedure 32
3.4.1 Transparent pipe test 32
3.4.2 MPRO test 33
3.4.3 Rheology measurement 36
3.4.4 Hot rolling 37
4. Result and discussion 38
4.1 System modification 38
4.2 Rheology measurement 39
4.3 Reference samples 42
4.4 Real samples 51
4.3.1 Water-based mud (WBM) 51
4.3.2 Oil-based mud (OBM) 54
5. Conclusion 57
Unsolved question 58
References 59

List of Figures

FIGURE 2- 1: LOW-SOLIDS OIL-BASED MUD WITH BARITE LEFT ON THE SCREEN AFTER ONE MONTH (TAKEN FROM TAUGBØL ET AL., 2005). 3
FIGURE 2- 2: CASING COLLAR STUCK IN CUT-PULL OPERATION(VRÅLSTAD ET AL., 2019) 4
FIGURE 2- 3: PARTICLE SETTLEMENT SCHEMATIC UNDER DIFFERENT FORCES (HAGHIGHI, 2015) 4
FIGURE 2- 4: HINDERED AND BOYCOTT EFFECT (ZAMORA, 2009) 7
FIGURE 2- 5: STATIC BOYCOTT SETTLING IN ZAG TUBE (ZAMORA, 2009) 8
FIGURE 2- 6: DYNAMIC BARITE SAG WINDOW (W DYE ET AL., 1999) 10
FIGURE 2- 7: DYNAMIC BARITE SAG COMPARED TO VISCOSITY PROFILE (W DYE ET AL., 1999) 10
FIGURE 2- 8: DRAG COEFFICIENT FOR THE DIFFERENT PROJECTED AREAS AND DIFFERENT SHAPES (NASA) 12
FIGURE 2- 9: TWO OIL-BASED MUD WITH THE SAME VISCOSITY AND DIFFERENT CLAY TYPE (TOR HENRY OMLAND, 2009) 14
FIGURE 2- 10: THE EFFECT OF ULTRASONIC VIBRATION ON SAG WEIGHT MEASUREMENT IN DIRECT METHOD (FARD ET AL., 2007) 15
FIGURE 2- 11: SETTLE PARTICLE WEIGHT IN STATIC AND DYNAMIC CONDITION (MAXEY ET AL., 2009) 16
FIGURE 2- 12: EFFECT OF PARTICLE SIZE DISTRIBUTION ON SETTLING RATE (T. H. OMLAND ET AL., 2007) 16
FIGURE 2- 13: STATIC SAG TEST FOR VERTICAL AND INCLINED CASE (BASFAR ET AL., 2020) 17
FIGURE 2- 14: SEGMENTS IN FLUID COLUMN (OMLAND ET AL., 2004) 17
FIGURE 2- 15: SAG SHOE , VST TEST (TOR H OMLAND ET AL., 2007),(BASFAR ET AL., 2020) 18
FIGURE 2- 16: FLOW-LOOP TEST (HANSON ET AL., 1990) 19
FIGURE 2- 17: FLOW-LOOP TEST IN DIFFERENT INCLINATION (HASHEMIAN ET AL., 2014) 20
FIGURE 2- 18: FLOW-LOOP TEST IN DIFFERENT ROTATION (HASHEMIAN ET AL., 2014) 20
FIGURE 2- 19: 1 D PROFILE FOR OIL-BASED SAMPLE (RISMANTO & ZWAAG, 2007) 22

FIGURE 3- 1: TRANSPARENT PIPE 23
FIGURE 3- 2: ADVENTURER BALANCES OHAUS 24
FIGURE 3- 3: MECHANICAL PROPERTIES ANALYZER 25
FIGURE 3- 4: HEI-TORQUE 400 (MIXER) 26
FIGURE 3- 5: HIGH-TEMPERATURE ROLLER OVEN 26
FIGURE 3- 6: HIGH-TEMPERATURE AGING CELL 27
FIGURE 3- 7: OFITE MODEL 900 VISCOMETER 28
FIGURE 3- 8: SAMPLES SETTLEMENT IN WITH DIFFERENT XG CONCENTRATION 29
FIGURE 3- 9: BARITE AND XG MEASUREMENT 31
FIGURE 3- 10: FLUID MIXING 31
FIGURE 3- 11: TRANSPARENT PIPE SCHEMATIC 32
FIGURE 3- 12: LAB VIEW LOGGIN 33
FIGURE 3- 13: VESSEL INNER SURFACE GREASING 33
FIGURE 3- 14: FILLING LEVEL GAUGE 34

FIGURE 3- 15: SIGNAL CABLES AND CONNECTORS 34
FIGURE 3- 16: PRESSURE APPLIED TO THE SYSTEM 35
FIGURE 3- 17: RESULT LOGGED FROM THE MECHANICAL PROPERTIES ANALYZER(ARROW, 2015) 35
FIGURE 3- 18: CUP CAPACITY 36
FIGURE 3- 19 : HOT ROLLING 37

FIGURE 4- 1: BUOYANCY EFFECT 38
FIGURE 4- 2: SHEAR STRESS-SHEAR RATE FOR REFERENCES SAMPLES 40
FIGURE 4- 3: SHEAR STRESS-SHEAR RATE FOR WATER-BASED MUD 41
FIGURE 4- 4: SHEAR STRESS-SHEAR RATE FOR OIL-BASED MUD 42
FIGURE 4- 5: TRANSPARENT PIPE TEST FOR REFERENCE SAMPLES 43
FIGURE 4- 6: DIRECT MEASUREMENT (HINDERED EFFECT) 43
FIGURE 4- 7: PARTICLE SETTLING SCHEMATIC FOR 0.6 GR XG 44
FIGURE 4- 8 : PARTICLE SETTLING SCHEMATIC FOR 0.9 GR XG 44
FIGURE 4- 9: PARTICLE SETTLING SCHEMATIC FOR 1.2 GR XG 44
FIGURE 4- 10 INDIRECT MEASUREMENT (BOYCOTT EFFECT) 44
FIGURE 4- 11 : REGRESSION ANALYSIS AND CURVE FITTING 45
FIGURE 4- 12: MPRO TEST FOR REFERENCE SAMPLE WITH 0.6 GR XG 46
FIGURE 4- 13: MPRO TEST RESULT FOR 0.6 GR XG IN HIGH RESOLUTION 46
FIGURE 4- 14: VISIONARY DRAWING EFFECT OF THE SETTLEMENT ON TRANSIT TIME 47
FIGURE 4- 15: COMPARISON OF MPRO TEST AND TRANSPARENT PIPE TEST RESULT FOR 0.6 GR X 47
FIGURE 4- 16: MPRO TEST RESULT FOR REFERENCE SAMPLE WITH 0.9 GR XG 48
FIGURE 4- 17: MPRO TEST RESULT IN LOW RESOLUTION FOR 0.9 GR XG SMAPLE 49
FIGURE 4- 18: COMPARISON OF MPRO TEST AND TRANSPARENT PIPE TEST RESULT FOR 0.9 GR XG 49
FIGURE 4- 19: MPRO TEST RESULT FOR REFERENCE SAMPLE WITH 1.2 GR XG 50
FIGURE 4- 20: MPRO TEST RESULT IN LOW RESOLUTION FOR 1.2 GR XG SAMPLE 50
FIGURE 4- 21: COMPARISON OF MPRO TEST AND TRANSPARENT PIPE TEST RESULT FOR 1.2 GR XG 51
FIGURE 4- 22: TRANSPARENT PIPE TEST RESULTS FOR WATER-BASED MUD 52
FIGURE 4- 23 : REGRESSION ANALYSIS AND CURVE FITTING 53
FIGURE 4- 24: MPRO TEST RESULT FOR WATER-BASED MUD 53
FIGURE 4- 25: MPRO AND TRANSPARENT PIPE TEST RESULT COMPARISON FOR WATER-BASED MUD 54
FIGURE 4- 26: TRANSPARENT PIPE TEST RESULTS FOR THE OIL-BASED METHOD 54
FIGURE 4- 27: REGRESSION OF TRANSPARENT PIPE TEST RESULTS FOR OIL-BASED MUD 55
FIGURE 4- 28: MPRO RESULT FOR OIL-BASED MUD 56
FIGURE 4- 29: MPRO AND TRANSPARENT PIPE TEST RESULT COMPARISON FOR OIL-BASED MUD 56

List of Tables

TABLE 2- 1: INVERT-EMULSION COMPONENT (TOR H OMLAND ET AL., 2004) 13
TABLE 2- 2: SAG FACTOR AND DYNAMIC SEDIMENTATION INDEX (SD) OMLAND ET AL., (2004) 13
TABLE 2- 3: FLUID COMPOSITION (TOR HENRY OMLAND, 2009) 14
TABLE 2- 4: FLUID COMPOSITION WITH 1.2 SG VISCOSITY (MAXEY ET AL., 2009) 15

TABLE 3- 1: FOUR DIFFERENT RECIPE FOR FLUID SAMPLE 29
TABLE 3- 2: OBM INGREDIENTS 29
TABLE 3- 3: WBM INGREDIENTS 30

TABLE 4- 1 : SHEAR STRESS-SHEAR RATE VALUES FOR REFERENCE SAMPLE 39
TABLE 4- 2: SHEAR STRESS-SHEAR RATE VALUES FOR WATER-BASED MUD 40
TABLE 4- 3: SHEAR STRESS-SHEAR RATE VALUES FOR OIL-BASED MUD 41

1. Introduction

Barite sag is a slow settlement phenomenon in fluid due to gravitational force, damage, or degradation of polymers in drilling fluid, which separates the particles from the liquid phase and result settle out of the suspension and lead to a variation of density.

Barite settling can occur either during the static condition (e.g., RIH, POOH, etc.) or during circulation (known as dynamic barite sag). Direct and indirect methods measure particle settlement. Direct methods are defined in density units, and indirect measurement seeks to infer sag presence (Saasen et al., 1995). There are major drilling problems related to barite sag, including stuck pipe, kick, blow out, and issues related to the running casing. Drilling fluid is the primary well barrier element during drilling and well construction (Khalifeh & Saasen, 2020).

The direct method has not been practically experienced so far, but there are different indirect measurement methods such as UCA (ultra-sonic cement analyzer), which has been investigated (Mjølhus, 2011). Therefore, in this work, I am going to measure the barite sag in the direct method and try to find a correlation between direct and indirect methods.

1.1 objectives

The main objective of this work is the direct measurement of barite particle settling in drilling fluids and correlating it with the indirect measurement method. The direct measurement was done by measuring the sedimentation rate of a reference system. At the same time, the changes in acoustic signal travel time occurred due to barite settling can be monitored by compressional wave velocity measured by utilizing a Mechanical properties analyzer (MPro). Then, the compressional wave will be coordinated to direct measurement to see there is any correlation between direct and indirect measurement. We assume that there is a change in the velocity of the compressional wave in fluid when the barite particles settle out of the drilling fluid at static conditions. To address the objective, a simple xanthan gum fluid with barite content is used as reference and our system is calibrated. In the next step, water-based and oil-based fluids are used to quantify the intensity of barite sag and reliability of the developed system.

2. Literature Review and Background Theory

2.1 The Effect of particle settlement barite on completion and drilling fluid

Drilling fluid has significant rolesin drilling operations such as wellbore stabilization, cutting removal and transformation, drill string, and bit lubrication. Another prominent role of drilling fluid is keeping the wellbore pressure over the formation pressure to prevent kick and blow-out incidents. Drilling fluid is also needed to transfer the cutting from the bottom hole to the surface. During well construction, high-density fluid will be necessary to ensure well control and wellbore stability. For this purpose, drilling fluid density is increased by weighting material additives such as bentonite, barite, ilmenite, magnetite, siderite, calcite, manganese tetraoxide, and salts. Barite is a well-known agent which has high density and low toxicity. Barite is chemically inert and insoluble. It occurs as a vein filling and as a gangue mineral in silver, zinc, copper, nickel, and lead ores (Labastie, 2011).

After a long production time, drilling in a reservoir that has been depleted can be a big challenge due to the small operational pressure window. Fracture pressure will be decreased due to the depletion. Some techniques to maintain fracture strength has been proposed (Morita et al., 1990). Weighting material such as barite can be added to the fluid to fill the fractures and prevent fracture propagation. Then, formation strength will be increased.

The primary mechanism, which causes more strength for formation is the arching phenomenon (Walker, 1966). In the arching phenomenon, open fractures are plugged when the particles have a size distribution. However, the settlement of particles such as barite causes variation in size distribution, disturbs formation strength enhancement. In the last phase of drilling operation into the reservoir, the fluid is displaced by completion fluid. It is necessary to have a completion fluid with appropriate barite content to provide a good filtration. This filtration avoids migrating unwanted fluid into the formation. But filtration will be influenced if there is not good size distribution due to the barite settlement (van der Zwaag et al., 1997).

As shown in Figure 2. 1, weighting material settlement in the screen can be a severe problem during production (Taugbøl et al., 2005). Different parameters such as viscosity and particle size can affect on-screen plugging.

Figure 2- 1: Low-solids oil-based mud with barite left on the screen after one month (Taken from Taugbøl et al., 2005).

The tendency of barite to sag is high, and it needs viscosifiers and gellants to keep the particle suspended and make it easy for distribution and prevent it from settling. Barite settlement can cause some problems from drilling operation step to plug and abandonment procedure.

Barite sag can decrease the fluid density near the surface during drilling and increase the density in fluid close to the bottom, which causes a non-linear hydrostatic pressure gradient. The other problems which occur due to the barite sag in drilling operation are lost circulation, well control, poor cementing and stuck pipe, casing, and logging tools.

In the subsequent phases, such as production and injection, there is another challenge regarding barite, which is scale. Variation in some main parameters in a system like pressure and temperature can result in scale. In this phenomenon, water formation with high barium mix with seawater, which is injected into the reservoir for pressure maintenance, leads to settling barium sulfate and scale accumulation.

The scale can occur during the production of multiple zones if the different fluid of zones mixes, which have sulfate and barium. The negative effect of the barite scale can be production losses.

Barite scale can lead to another difficulty during well abandonment. In cut-and-pull operation (Khalifeh & Saasen, 2020), it is possible to experience casing stuck due to settled barite behind

casing in the annular, which occurred in a long time when the well is in static condition. In this situation, barite is separated and settled due to the gravitational force and accumulated in the annulus.

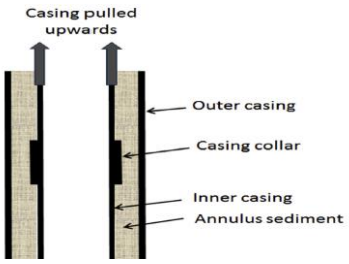

Figure 2- 2: Casing collar stuck in cut-pull operation(Vrålstad et al., 2019)

2.2 Basics of settlement

In particle settling, if the mass of particle which is subjected by gravitational force (Fg) and drag force (Fd) is *m* and density of the fluid is ρf, based on second newton's law we have :

$$F_g - F_d = m\frac{dv}{dt} \quad \text{Eq.1}$$

where *v* is settling velocity.

Reynolds number can be defined based on apparent viscosity (η) :

$$Re = \frac{v^2 r\, \rho f}{\eta} \quad \text{Eq.2}$$

Figure 2. 3 indicates the different forces applied on the particle during settlement.

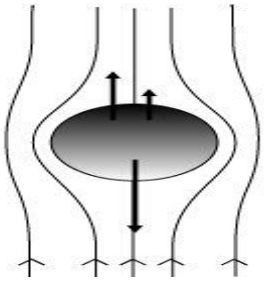

Figure 2- 3: Particle settlement schematic under different forces (Haghighi, 2015)

The frictional drag force (Fd) is expressed by :

$$Fd = \frac{1}{2} C_D\, \rho f\, vt^2 A \quad \text{Eq.3}$$

And for spherical particle with radius (r) is expressed by :

$FD = 6\ \pi\ \eta\ r^2$ Eq.4

where A is particle surface area, the C_D is drag coefficient, and *v*t in Eq.3 is terminal velocity and can be derived by stokes law (Stokes, 1901):

$$Vt = \frac{2r^2 g(\rho p - \rho f)}{9\eta}$$ Eq.5

Then settling velocity can be defined by the Stokes equation. It is necessary to mention that as a limitation in stokes law; it is valid for particles with Reynolds number less than one (Re < 1) (C. K. Batchelor & Batchelor, 2000).

2.3 Barite sag

Barite sag is the variation in mud density when the weighting materials are settled in downhole (Bern et al., 1998). Barite sag is a complex phenomenon in drilling. Although there are many years in which it has been investigated, there is no clear definition of sag.

In one of the previous investigations, sag detection has been developed in rig site (Bern et al., 2010). In that work, barite sag is defined so that weight-material sag has occurred when there is drilling fluid density variation of more than 0.5 lbm/gal in the static condition where the fluid has no circulation for a long time in inclined well. As it is mentioned, the dynamic condition also leads to barite sag when the drilling fluid is in motion. In directional drilling in a curved well, when the pump is off and the circulation rate is low in the static period, the particle settled in the range of high to the downside of the hole. Density variation in the sagging bed is down due to the gravitational effect, making pressure imbalance. The force caused by imbalance pushes drilling fluid with low density to up and accelerates the particle settling known “boycott effect”. with increasing the particle settlement, the boycott effect amplifies the downward flow of barite sag is called avalanche. With increasing the inclination of the wells (high-angle) wells barite sag is intensified regarding increasing the particle settling rate. Regarding the rheological aspect, barite sag occurs when there are no sufficient properties to keep the weighting agent suspended, which leads to the high-density slurry and barite bed on the lower side of curvature in well. When the pump is on, it is challenging to recirculate the drilling fluid since fluid density, viscosity, and gel strength of the lower part of the well where the sag occurs are increased. Hydraulic pressure at the higher part of the well will be decreased during low barite concentration, which results in collapse, kick, and water, oil, and gas influx.

2.4 Mechanisms of barite settlement

It was assumed that barite sag occurred only in static condition since deposit lamination were identified in directional wells in a long time. Afterward, (Hanson *et al.*,1990) discovered the effect of dynamic conditions on barite settlement. Laboratories investigations claimed that barite deposit formed during circulation and will be increased in the static condition, which leads to density variation in fluid column. Using an inclined flow loop in the laboratory, density variations in axial and cross-sectional directions were calculated.

2.4.1 Static condition (Boycott and Hindered effect)

Further, it was found that the rate of particle settlement in the fluid is higher in inclined pipe compare to the vertical pipe, and the reason is related to a phenomenon which first has been discovered by (Schaflinger, 1985). He noticed that the blood corpuscle settled in an inclined tube faster than the vertical type. This Boycott effect was found during investigations in drilling fluids. During particle settlement in inclined annulus or pipe, fluid with low density is moved upward, and high-density fluid moves down on the downside of the well. Pressure imbalance due to this phenomenon leads to make fluid movement faster.

Figure 2.5 (Zamora, 2009) illustrates the particle settlement in vertical and inclined profiles. In both cases, suspended particles are denser than suspending fluid settle with V0 velocity due to gravity.

In hindered effect, shown on the left side of Figure 2.4 in a vertical pipe, there are three different zones for particle settlement. In this effect, particle concentration increases from top to bottom. The zones are defined as :

- Clarification zone: there is free settling, and based on stokes' law, particles settle individually.
- Hindered settling zone: with increasing the concentration of surrounding particles, settling individual particles will be disturbed, and the settling rate is lower than free settling. If the particles form clusters and get bigger, the settling rate will increase due to their size.
- Compaction regime: with increasing the concentration at the bottom of the pipe, the fluid will be extracted and barite bed compacts.

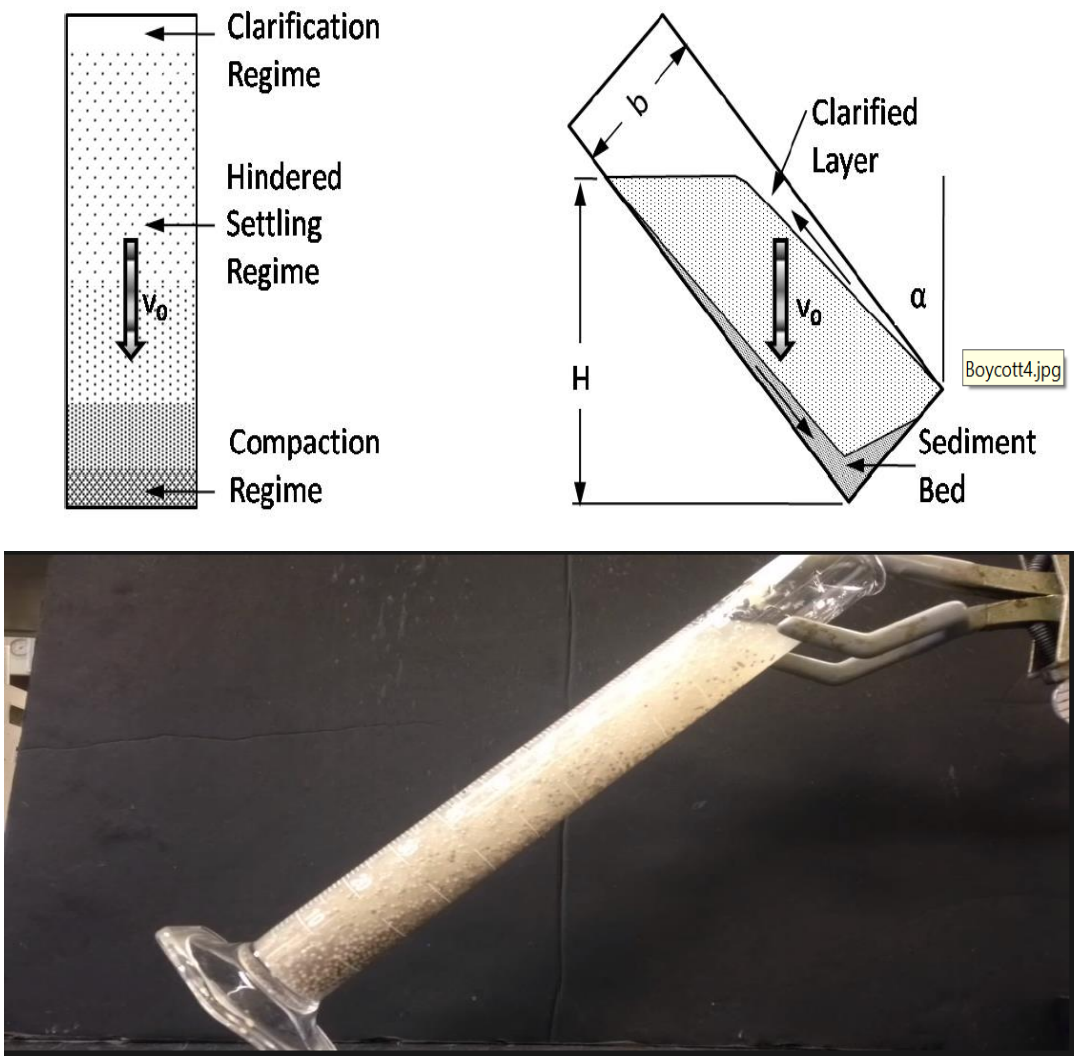

Figure 2- 4: hindered and boycott effect (Zamora, 2009)

It is necessary to mention that one of the factors that can affect on hindered effect is moving the displaced fluid upward and make it possible to settle the particle quickly.

The right side of Figure 2.4 shows the particle settlement in the inclined tube. In this shape, there is a short distance for particles to settle down during vertical settlement. Regarding the buoyancy effect, the clarified layer flowed upward and occurred on the top side of the tubing. With increasing the particle settlement, sediment bedforms in the low side of the tube, which leads to slump to the bottom of the tube and avalanche phenomenon, results in a high concentration of particles. The critical angle for avalanche with severe slumping is 45 degrees. When the inclination is more than 45 degrees, the buoyancy effect decreases, which causes a low settling rate. PNK model (NAKAMURA, 1937) (Ponder, 1925) has been defined for boycott modeling, which is validated by numerous experimental studies in particle settlement between parallel plates:

$$S(t) = vo \frac{b}{\cos(\propto)} \left[1+\frac{H}{b}\sin(\propto)\right] \quad \text{Eq.6}$$

$$\frac{dH}{dt} = -vo \left[1+\frac{H}{b}\sin(\propto)\right] \quad \text{Eq.7}$$

Where :

S(t) : effective settling rate , α : inclination

V(0): particle settling velocity (can be defined as slip velocity in drilling fluid)

H(t): immediate suspension height, H: suspension height

Zag tube is training equipment that shows the hindered and boycott phenomenon. There are different sizes of this equipment. Figure 2.5 indicates particle settlement in the Xanthan-gum solution. The left side picture in Figure 2.5 shows different zones, which are already described in detail.

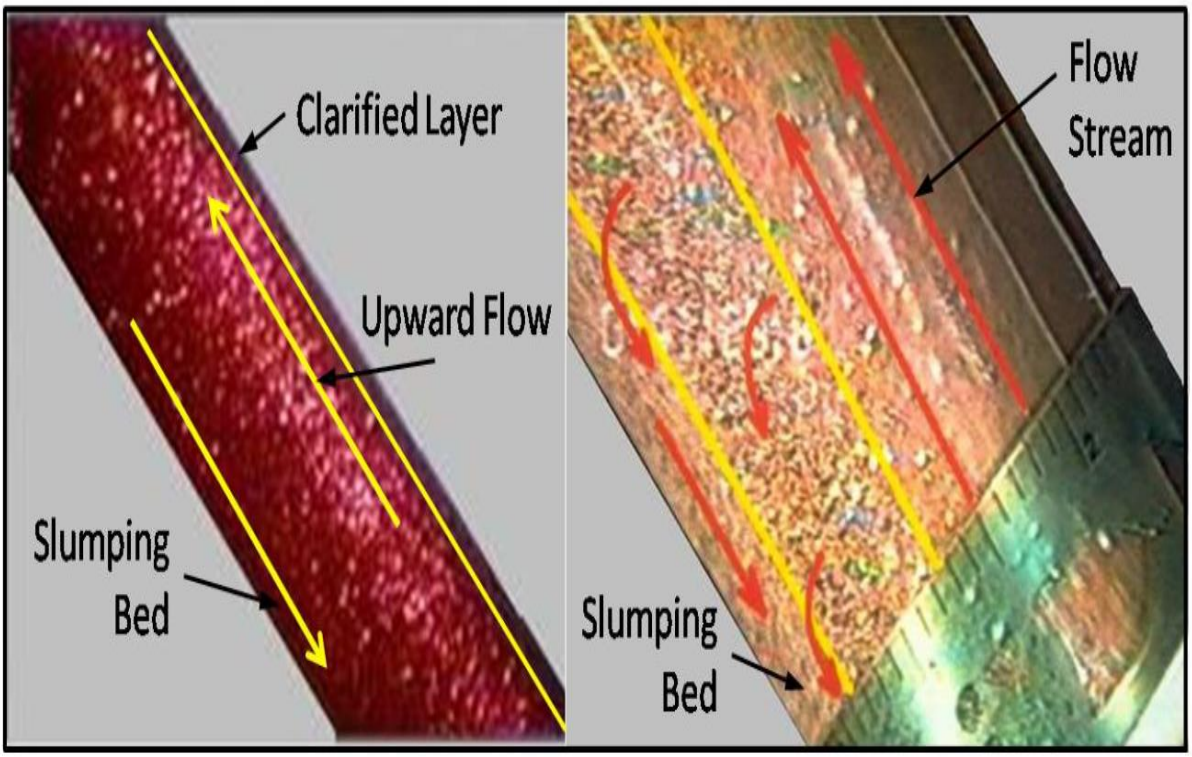

Figure 2- 5: static boycott settling in zag tube (Zamora, 2009)

As the figure shows, a flowing stream occurred in the upper half of the tube. The middle zone (upward flow) appears gradually and pushes the particles to the slumping bed. Then the slumping bed is force opposite of flow with higher velocity than static suspension.

"Accelerated" boycott settling is the crucial concept that can amplify barite sag in flow rate. With decreasing the flow rate, gels are already broken, and viscosity will be reduced in the shear-thinning fluid, which causes sag severity. The Boycott effect is essential in this study

because the Mpro (indirect measurement) technique involves the Boycott effect, while the direct technique used in this study considers the Hindered effect.

2.4.2 Dynamic condition

In dynamic conditions, which is one of the settlement mechanisms, it was shown that preventing sag is more complicated, and dynamic sag has more importance and complexity (Saasen et al., 1995). In earlier works (Kenny et al., 1994), based on Newtonian suspension, they found that in fluid with higher viscosity, there is lower dynamic sag. Settlement can exist very fast in a fluid with high gel strength in dynamic conditions. In this condition, during fluid circulation, the fluid may have high gel strength, and still, dynamic sag occurs since the fluid has lower shear. This can be the same in annulus space between casings with low rotation, while in other studies (Tor Henry Omland, 2009), it has shown that there is a higher settlement rate with increasing the rotation.

2.4.3 The effects of particle properties and fluid rheology on settlement

There are several studies that investigated the operational and rheological effect of fluid on barite sag and particle settlement (Dye et al., 1999, W Dye et al.).

They found that low shear rate viscosity is the main critical rheology parameter for dynamic barite sag. They stated dynamic sag occurs at the low shear rate (3 rpm) when dial reading is 5.1 s^{-1} which is the lowest operating speed of the Fann viscometer. (William Dye et al., 1999) demonstrated that viscosity measurement taken at ultra-low shear rates ($< 2s^{-1}$) correlates with decreasing dynamic barite sag potential.

The dynamic sag window was presented by (W Dye et al.,1999) where identical shear rate barite sag and rotational viscosity were measured. This tool was introduced to predict dynamic barite sag potential with ultra-low shear rate viscosity measurement. Rotational viscosity evaluation to the limit of dynamic sag window could predict dynamic barite sag potential since dynamic barite sag and rotational viscosity was measured at the same shear rate. Fig 2.6 and Fig 2.7 illustrate the limitation of dynamic barite sag and its potential based on viscosity. Some operational parameter effects were discovered, so that found dynamic barite sag generally increased when hole inclination change from 45° to 60°.

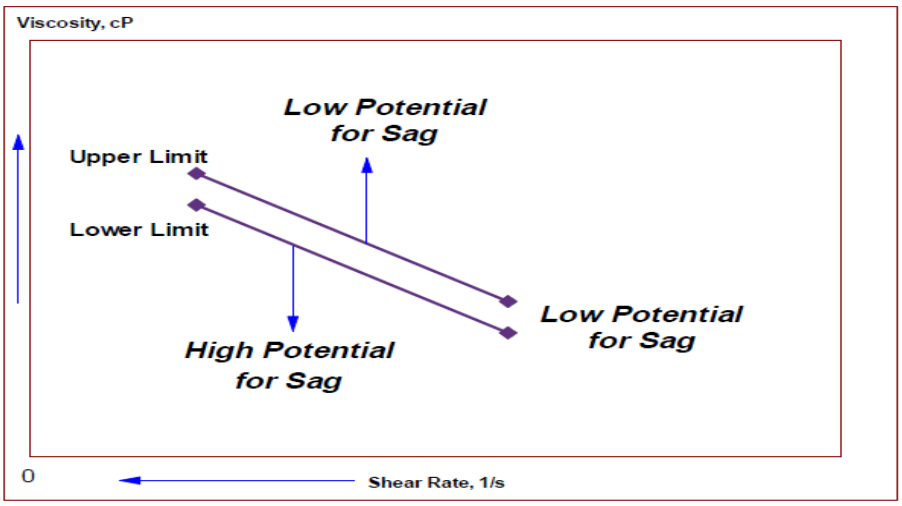

Figure 2- 6: Dynamic barite sag window (W Dye et al., 1999)

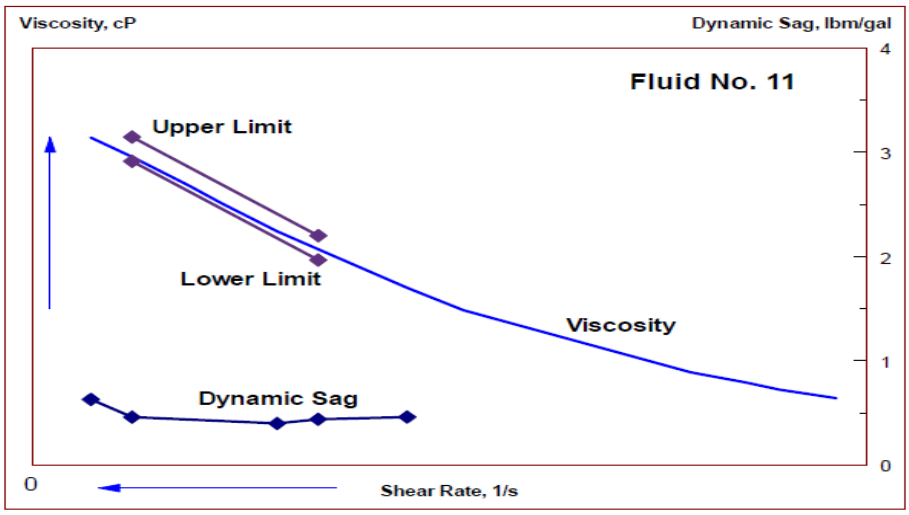

Figure 2- 7: Dynamic barite sag compared to viscosity profile (W Dye et al., 1999)

Mentioned studies also stated when annular velocity in the well is higher than 100 ft/min, dynamic sag levels were low, and at low shear rate conditions, ultra-low shear rate viscosity compensated the reducing effect of high velocity.

(Basfar et al., 2020) studied the temperature effect on static and dynamic sag. The results from different experiments on fluids (including barite with copolymer and without additive) indicate increasing the temperature leads to a higher sag factor.

Some factors are related to the fluid density effect on sag (Saasen, 2002). The density of the mixture is equal to the fluid when the particles settle ultimately. During particle settling, when a particle has movement, a counter flow of fluid is accrue to fill the volume of particle which has been replaced. Limitation of weighting material amount, which indicates low density leads

to an inadequate velocity of counter flow. High particle concentration, which means high fluid density causes settling of large weight material volume and then it results in more volume of replaced flow. Resistance toward settling movement increases due to the high fluid density. (William Dye et al., 1999) calculated the water-based fluid density, which leads to most sag severity and is equal to 1.55 sg. If there is gel formation in the drilling fluid, the gravity force should break the gel formation prior to static sag. The force which is needed to break the gel formation is defined by :

$$F = \tau g \, Ap \qquad \text{Eq 8}$$

Where τg is gel strength, and Ap describes the surface area of particles. To break the gel formation, gravity force should be the domain of buoyancy force. Then the resultant force is :

$$F\text{- buoyancy force} = \Delta\rho \, VP \, g \qquad \text{Eq 9}$$

Where $\Delta\rho$ is the density difference between particle and fluid, VP is particle volume, and g is the gravitational acceleration.

Regarding Eq 8, gel strength which is needed to prohibit sag can be described by :

$$\tau g \geq \frac{\Delta\rho}{6} gD \qquad \text{Eq 10}$$

For example, for API standard barite with 25 microns, the gel strength which can prevent sag is equal to 0.13 pa (Fjogstad et al., 2000).

Different shapes of particles may affect the settling rate. The drag force given in Eq 3 is affected by particle shape. Figure 2.8 is provided by NASA, which illustrates different drag coefficients for various forms. The particles with the same mass, density, and total surface area have different settlement rates since they have different shapes.

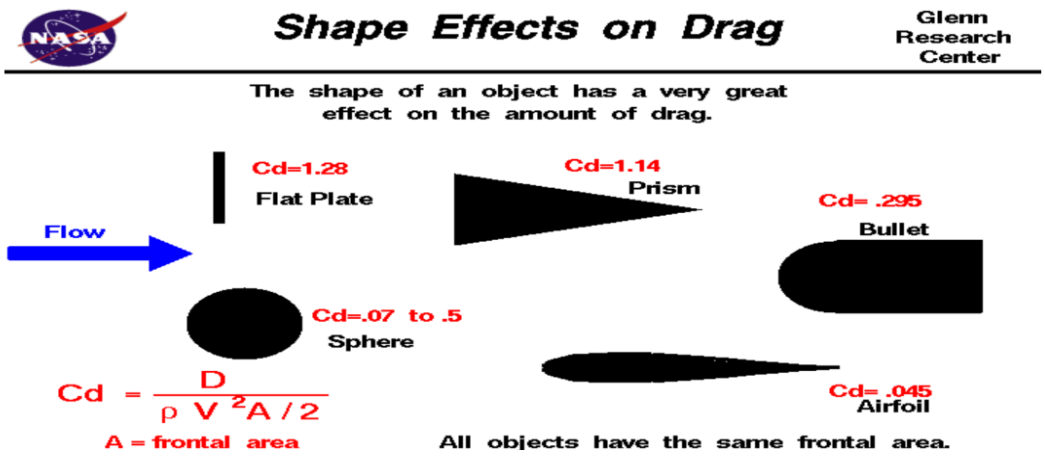

Figure 2- 8: Drag coefficient for the different projected areas and different shapes (NASA)

It is necessary to mention that the drag coefficient is not entirely constant and changes with settling speed like Reynolds number. For example, the drag coefficient for a sphere falling in the air is 0.47 at laminar conditions and is 0.1 at turbulent conditions.

Conformity, the work of stokes (Harriott & Barnstone, 1967) introduced drag coefficient model for Newtonian fluid as a function of Re:

$$CD = \frac{24}{Re}(1 + 0.186\,Re^{0.6459}) + \frac{0.4251}{1+\frac{6880.95}{Re}} \qquad \text{Eq 11}$$

Eq 12 indicates the drag coefficient for non-Newtonian fluid derived by (G. K. Batchelor & Wen, 1982) based on experiments.

$$CD = \frac{24}{Re}(1 + 0.1407\,Re^{0.6018}) + \frac{0.2118}{1+\frac{0.4215}{Re}} \qquad \text{Eq 12}$$

The models are based on empirical approximations and used for single spherical particle settlement.

(Omland et al., 2004) investigated how the different degrees of mixing energy and shear devices affect sedimentation potential of weighting material. They mentioned that there is more sag possibility in invert-emulsions compare to the water-based drilling fluids. Mixing of a barite phase with a continuous phase leads to an invert-emulsion drilling fluid. Table 2.1 illustrates the invert-emulsion fluid composition.

Table 2- 1: Invert-emulsion component (Tor H Omland et al., 2004)

Component	Function	Concentration
Base Oil	Cont. phase	580 l/m^3
Water	Disp. phase	150 l/m^3
Carboxylic Acid	Emulsifier	20-30 l/m^3
Salt	Formation salinity	30-50 kg/m^3
Organo. Clay	Viscosifier	5-15 kg/m^3
$CaCO_3$/ Polymer	Fluid Loss	10-100 kg/m^3
Weight agent.	Provide Density	880 kg/m^3

Two shear devices were used for experimental tests. One of them was producing pure shear unit to disperse the emulsion water droplets in the continuous oil phase, and another device was used to combine the shear and mixing unit. Based on stability measurement, there was a clear relationship between shear energy, rotational speed, and sedimentation potential. Based on sag measurement, table 2.2 indicates how the sedimentation potential changes with the number of cycles fluid pass through the shear zone, which means increasing the shear-energy reduces the sedimentation potential of weighting material in drilling fluid.

Table 2- 2: Sag factor and dynamic sedimentation index (SD) (Omland et al., 2004)

No. Circ	Stator/rotor Config	Speed (rpm)	Sag Factor	S_D
0	4-4-4-2	6000	0.538	0.559
8	4-4-4-2	6000	0.527	0.543
8	4-4-4-2	12000	0.518	0.526
1	2-2-2-1	12000	0.530	0.546
3	2-2-2-1	12000	0.519	0.530
8	2-2-2-1	12000	0.516	0.520

Stabilizing effect on the emulsion in particle settlement was investigated by organophilic clay additive. The emulsion consisted of oil, water, and brine phase based on cacl2. Electric stability increased by adding organophilic. In experiments, it is discovered that emulsion stability effect sag performance. As a result, if the brine droplet has the chance to unify, the density difference between the brine phase and continuous oil phase leads to settling. When some other force than gravity is implemented, there is not any settlement.

The effect of solid control on sag was mentioned by (Tor Henry Omland, 2009) in his thesis based on Mjølhus's thesis. To evaluate the effect, different tests with direct weight measurement conducted on samples. Table 2.3 indicates the composition of the first sample. Another sample was made to provide the viscosity by replacing the organophilic clay and bentonite addition and is more like drilling fluid includes drilling solids. The properties of the two samples were the same such as viscosity, but they had different sag stability

Table 2- 3: Fluid composition (Tor Henry Omland, 2009)

Component	Amount in 350 ml fluid
Base oil	268 ml
$CaCl_2$	78 ml
Primary emulsifier	11.7 ml
Secondary emulsifier	3.9 ml
$CaOH_2$ (Lime)	11.05 g
Organophilic clay	7.15 g
Fluid loss control agent	5.2 g
Barite	266.8 g

As it is illustrated in Figure 2.9, regarding experimental tests, sedimentation rates increased due to the Wyoming bentonite.

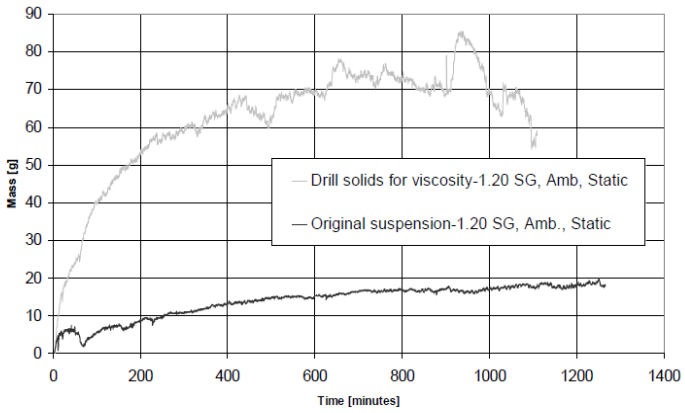

Figure 2- 9: Two oil-based mud with the same viscosity and different clay type (Tor Henry Omland, 2009)

(Fard et al.,2007) studied the effect of imposed vibrations on sag and shear stress. The investigation showed how the vibration leads to an increase in the settling rate due to the breaking gel structure of the fluid. In this experiment, an oil-based mud sample was put into an ultrasonic cleaning path. By using the static sag test method, which will be explained further,

the sag factor was measured. Figure 2.10 indicates the weight of settled material during the time. As it's seen in Figure 2.10, there is no significant difference between two samples with vibration and without in settlement rate, but after passing the time, there is a dramatic increase in settling when the sample is subjected to vibration.

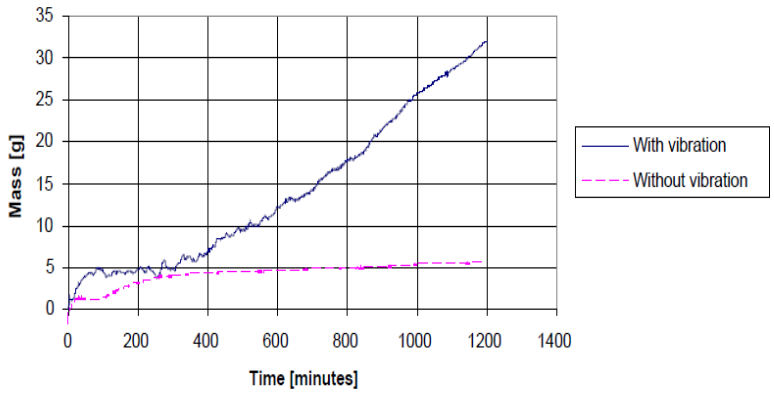

Figure 2- 10: The effect of ultrasonic vibration on sag weight measurement in direct method (Fard et al., 2007)

String rotation can influence settling rates in different well inclination. This effect was investigated by (Maxey et al.,2009) and (Omland et al.,2013) in an inclined and vertical well. They used a direct method for weight measurement. The tests were under ambient temperature with a different rotation. Table 2-4 shows the composition of the fluid sample, which made 1.2 SG fluid viscosity.

Table 2- 4: fluid composition with 1.2 SG viscosity (Maxey et al., 2009)

Component	Content
Base oil	268 ml
$CaCl_2$ (1.13 g/cm^3)	78 ml
Primary emulsifier	11.7 ml
Secondary emulsifier (wetting agent)	3.9 ml
$CaOH_2$ (Lime)	11.05 g
Organophilic clay	7.15 g
Fluid loss control agent	5.2 g
Barite	As required

As a reference, several static tests were performed. Figure 2.11 demonstrates the settlement rate at the static condition and different rotation. As it is seen, it can be concluded that settling rate increase due to the rotation.

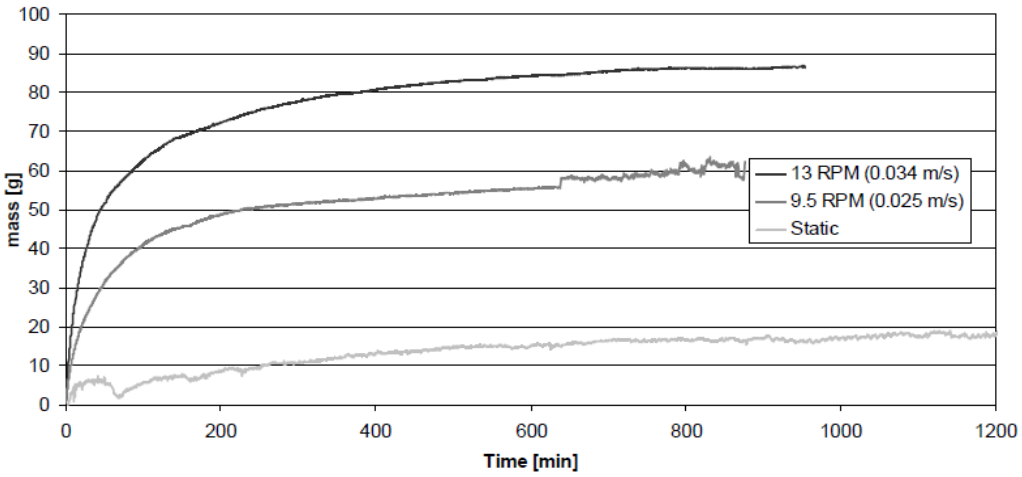

Figure 2- 11: Settle particle weight in static and dynamic condition (Maxey et al., 2009)

The particle size distribution (PSD) effect on sag and settlement was investigated (Omland et al.,2007). As shown in Table 5, two-fluid samples were prepared with different PSD included barite as a weighting material in their experiments. One sample had limited particle size distribution and the other had broader with identical density. A direct method for weight measurement was used in related tests. Figure 2.12 illustrates the effect of PSD on settling rate in the test which had 2 hr period. The result showed narrow particle size distribution has higher sag potential than broad distribution.

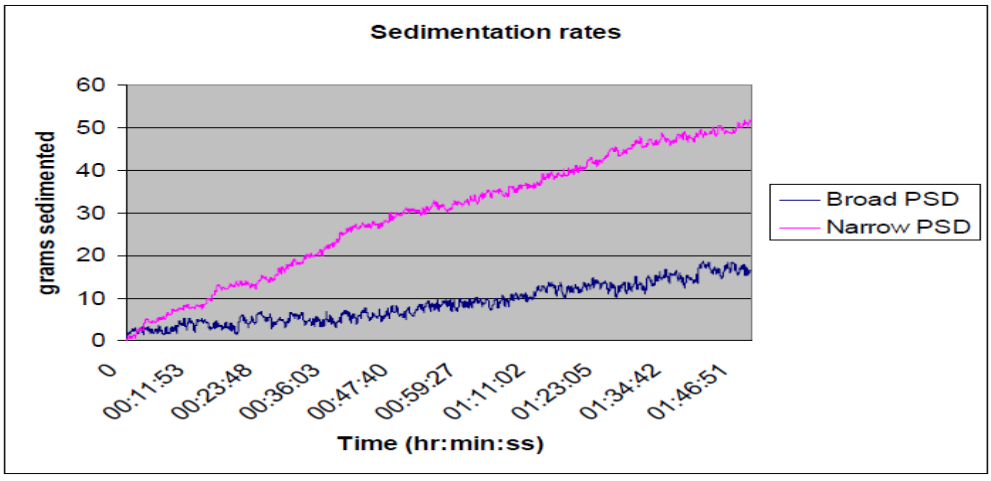

Figure 2- 12: Effect of particle size distribution on settling rate (T. H. Omland et al., 2007)

2.5 Barite sag measurement techniques

Several different techniques have been designed to measure the sag and settlement which used in the field and the laboratory. A wide range of instruments such as simple viscometer and

advanced equipment were used to investigate sag performance. In further, different methods will be explained, and in the next chapter, the direct measurement method which has been experienced in this study will be described in detail.

2.5.1 Static sag testing

In one ordinary method for sag measurement in the static condition, a steel cell gets filled by fluid and warmed up in oven in designed temperature for a term of time as it is indicated in figure 2.13 (Tor H Omland et al., 2007)

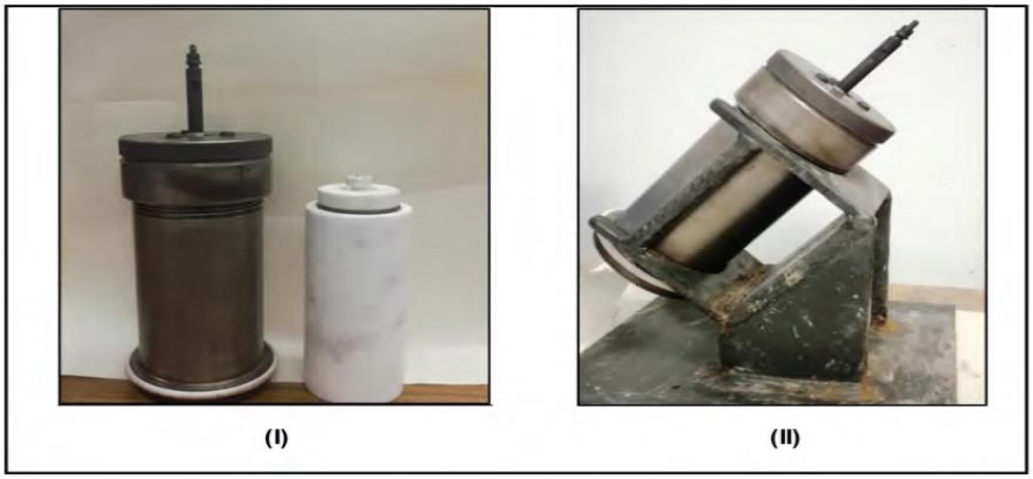

Figure 2- 13: Static sag test for vertical and inclined case (Basfar et al., 2020)

This test can be appropriate for the frequent test but is no useful for circulating conditions. The designed temperature is usually 100 ° C. The test takes 64 hrs (Omland et al.,2004), as Figure 2.14 illustrates, the whole fluid column is divided into one clear fluid, which is called the free layer, and four segments.

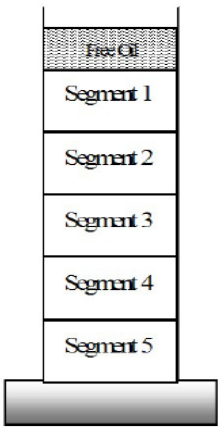

Figure 2- 14: Segments in fluid column (Omland et al., 2004)

The density of segments is different, and this difference can be useful to calculate sag tendency. Sag tendency is expressed by sag factor, which is illustrated in eq 13 (Tor H Omland et al., 2007),(Tor H Omland et al., 2004).

$$\text{Sag factor} = \frac{Mw\ bottom}{Mw\ bottom + Mw\ top} \qquad \text{Eq 13}$$

Where Mw bottom is the density of the bottom layer, and Mw top is top layer density. There is not any sagging fluid if the sag factor is equal to 0.5, while the sag factor higher than 0.5 leads to an operational problem. Free liquid on top of the column is removed by settling particles and is not considered in sag tendency. This method can not be very precise and suitable for the industry as a standard. The mentioned effect can be compensated by presenting a dynamic sedimentation index that demonstrates the immediate settlement of the initial drilling fluid (Omland et al.,2004). Eq 14 expresses dynamic sedimentation index:

$$S_D(t) = \frac{Mw\ bottom}{Two\ Mw\ initial} \qquad \text{Eq 14}$$

Where $S_D(0) = ½$, which means at initial condition density of fluid is uniform.

2.5.2 Viscometer sag testing

In order to sag measurement in dynamic conditions, a simple test was introduced, which is the viscometer sag test (VST) (Zamora et al., 2004). Standard measurements of this test are funnel viscosity (FV), yield point, and 100 rpm reading of a fan 35 viscometer. In this test, the thermocup is filled with mud, and after 30 minutes of shearing, the density at the top and bottom of thermocup is measured, and it can be an indicator of the measured densities are compared to the initial density. To improve the sensitivity of the standard viscometer sag test, it has been modified by a thermoplastic which is called “shoe,” and placed at the bottom of viscometer (Omland et al., 2007) (Basfar et al., 2020). As it is indicated in Figure 2.15, the settling rate is accelerated by the sloping surface of the shoe due to the boycott effect and weight material such as barite will be collected at the bottom of the thermocup.

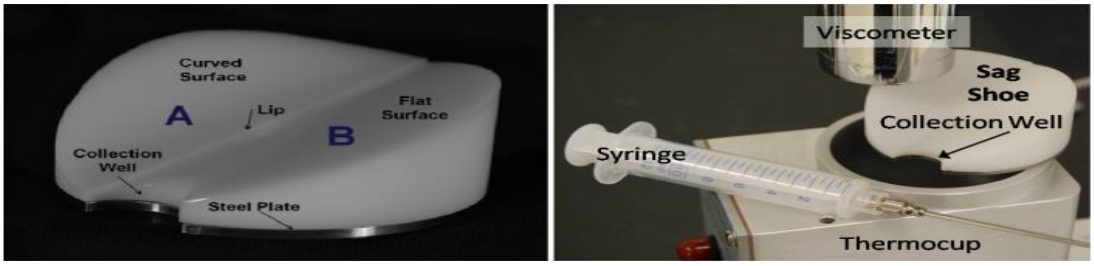

Figure 2- 15: Sag shoe , VST test (Tor H Omland et al., 2007),(Basfar et al., 2020)

Computational fluid dynamic (CFD) analysis was performed to compare the result of VST and viscometer sag shoe test (VSST) (Zamora et al., 2004). Sag tendency in this test is named "sag register," which is defined by Eq 15 :

$$S_R = -k \frac{\Delta Mw}{Mw} \qquad \text{Eq 15}$$

Where ΔMw is fluid density difference between two runs at the bottom of thermocup, Mw is initial fluid density, and K is an empirical constant which is 10.9 for (VSST) test. There is no sag if the sag register is equal to 1, while values below 1 indicate fluid sag (Tor H Omland et al., 2007).

2.5.3 Sag flow loop test

The sag flow loops provide a sag detection foundation and have a complex setup. This test needs high fluid volume and space for instrumentation, especially at the rig site. There are some limitations in the flow-loop test to simulate downhole conditions such as rotation effect, geometry, and temperature. one of the first flow-loop tests was conducted by (Hanson et al., 1990), and flow-loop studies were instrumental in identifying weights reported in the field. Figure 2.16 illustrates a large flow loop that was conducted to study the effects of drilling parameters on barite sag.

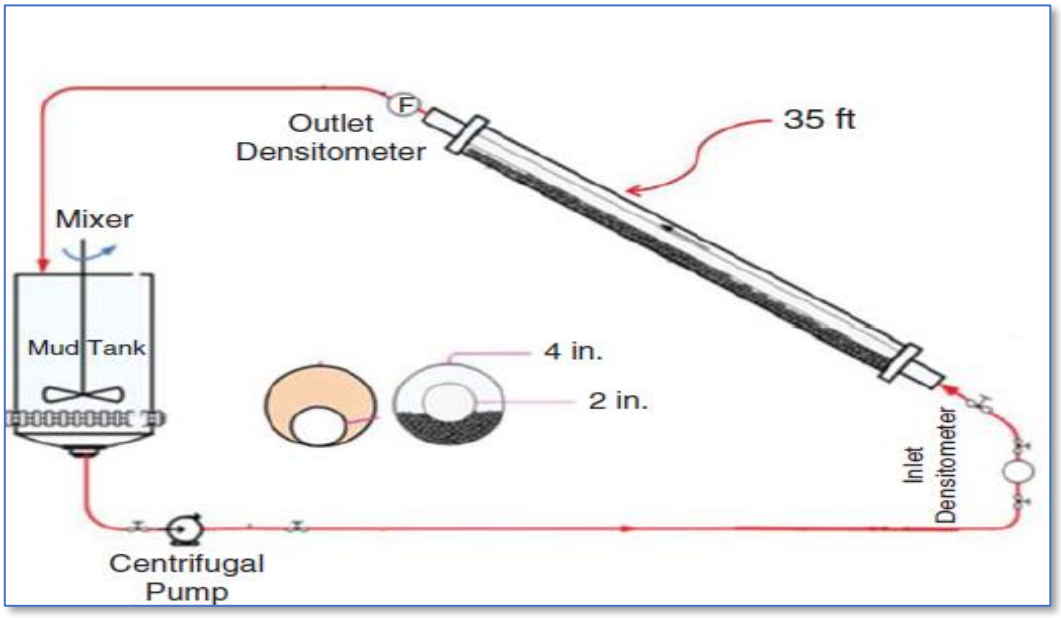

Figure 2- 16: Flow-loop test (Hanson et al., 1990)

The inclination of the test section changed from horizontal to vertical. As Figure 2.17 shows, decreasing the inclination leads to lower barite sag (Hashemian et al., 2014)

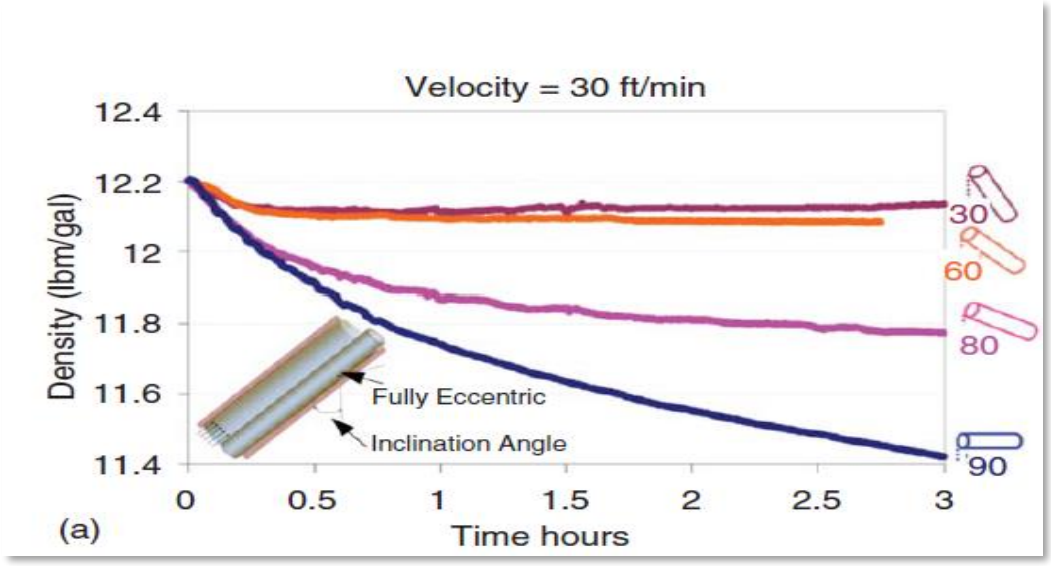

Figure 2- 17: Flow-loop test in different inclination (Hashemian et al., 2014)

Figure 2.18 indicates the effect of rotation on barite sag which was resulted by flow-loop test. Barite sag increases as the string rotation raises.

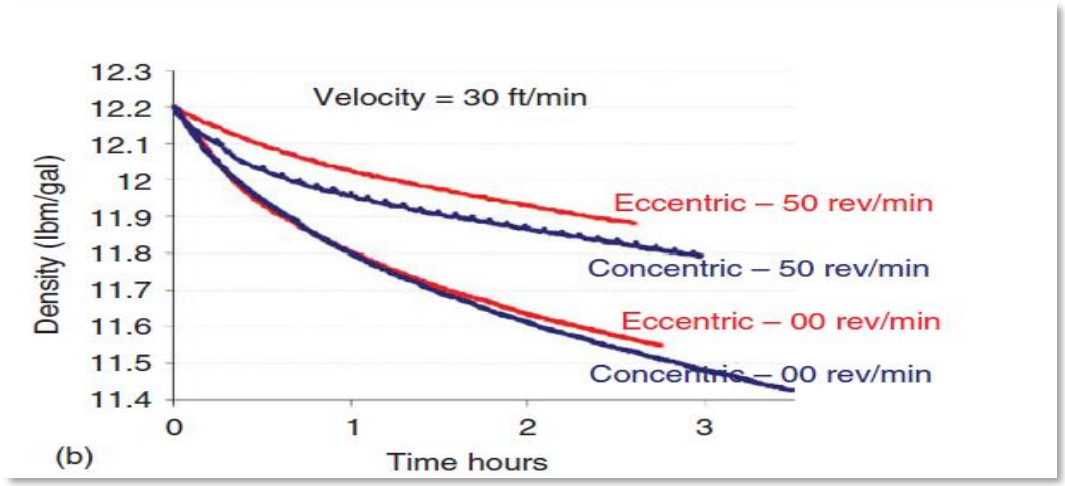

Figure 2- 18: Flow-loop test in different rotation (Hashemian et al., 2014)

2.5.4 High angle sag test

A high-angle sag test was conducted regarding some limitations for sag measurement in the flow-loop method (Jamison & Murphy Jr, 2003). More downhole conditions are simulated in this test, such as pressure, temperature, string rotation, and hole cleaning. The fluid sample is located in a pipe with desired angle, pressure, and temperature. Torque change in the shaft which holds the pipe indicates mass center shifting in the sample. During the settlement, mass measurement in the sample is monitored and plotted as a function of time which is expressed by Eq 16 (Tor H Omland et al., 2007).

$$X_{cm} = \left(\frac{At}{B+t}\right) \quad \text{Eq 16}$$

where A is the maximum mass movement and B is the time when the center of mass has movement in half of the maximum. Eq 17 indicates the sag coefficient and indicates the total sag which happens within the time and is derived by investigating the mass movement function.

$$Sc = \int_0^t X_{cm\,(t)}\, dt \quad \text{Eq 17}$$

when Sc is equal to zero, it indicates there is not any mass movement and not sag.

2.5.5 ultrasonic measurement

ultrasonic measurement was used to measure the concentration of slurry during solid settlement over time (Bamberger & Greenwood, 2004). They investigated sound speed, which was traveling through the sample, and how density variation affects sound propagation. The idea of this technique is based on signal reflection of ultrasonic and how sound wave is transfered in the sample and affected by particle shape, size, and concentration so that reflected energy depends on parameters which are mentioned above. (Mjølhus., 2011) investigated the particle sedimentation by ultrasonic cement analyzer (UCA). Different fluids have experimented including oil-based and water-based mud. UCA is commonly used for compressive strength tests of cement, but it was interesting if the velocity of ultrasonic sound transferring through the mud sample changed during the particle settlement and recorded as transit time by UCA.
In this experiment, the drilling fluid is poured into the high-pressure cell, and ultrasonic waves were applied through the fluid sample by UCA. The different parameter which could affect on ultrasonic wave were experienced such as vibration, temperature, fluid density, air bubble, emulsion stability, and pressure. The results suggested that settlement increases 4% when there are no vibration and transit time increases due to the air bubbles inside the sample.

2.5.6 Sag detection by nuclear magnetic resonance

The nuclear magnetic resonance technique usually is used to analyze the rock properties in the petroleum industry. During the measurement, there is not any contact with fluid in NMR method (Rismanto & Zwaag, 2007). Different types of fluid such as water-in-oil emulsion and oil-based drilling fluid with different oil-water content were performed. In this experiment, T1 and T2, which illustrate longitudinal and transverse relaxation time respectively, were measured in different oil-water content for both emulsions and oil-based mud. Another type of measurement was a 1D profile experiment performed on an oil-based mud sample in a static condition at specific pressure and temperature. The objective of the static condition was to monitor the barite settlement. The whole height of the fluid column was 6 cm. As it is shown in Figure 2.19, 0 cm height indicates the bottom of the fluid column, and 6 cm is the top of the column. Based on Figure 2.19, a high NMR signal reflects the pure liquid with low particles while the low signal is related to the liquid phase, which is affected by solid accumulation, and profiles are varied for different oil-water content.

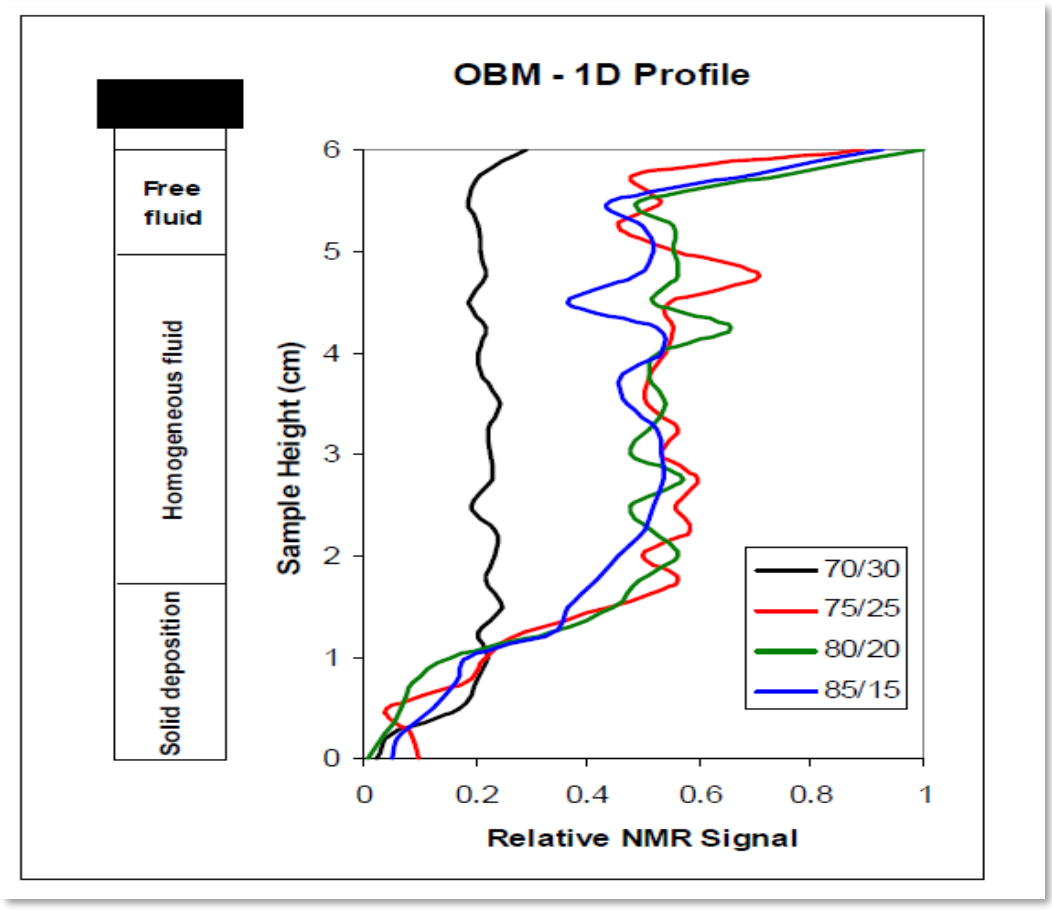

Figure 2- 19: 1 D profile for oil-based sample (Rismanto & Zwaag, 2007)

In this work, the direct method was used for barite sag weight measurement, which will be explained in detail in the following chapters. In this technique, the settling rate of the weight particles is monitored directly by a scale connected to the cup by a rod. The scale continuously records the suspended particles, which are separated from the liquid phase and falling into the cup. The collecting cup is inside the pipe and plunged in fluid when the transparent pipe is filled by sample.

3. Methodology and Experimental work

In this section, the chemicals used to prepare samples and the mixing procedure of drilling fluid are explained in detail. Different equipment required to test the samples will be presented, and several suggested recipes are labeled further.

3.1 Equipment

3.1.1 Transparent pipe

As shown in Figure 3.1, the transparent pipe used for this experimental work includes a glass pipe with 130 cm in length and 6 cm diameter held by a metal block to stabilize and prevent vibration.

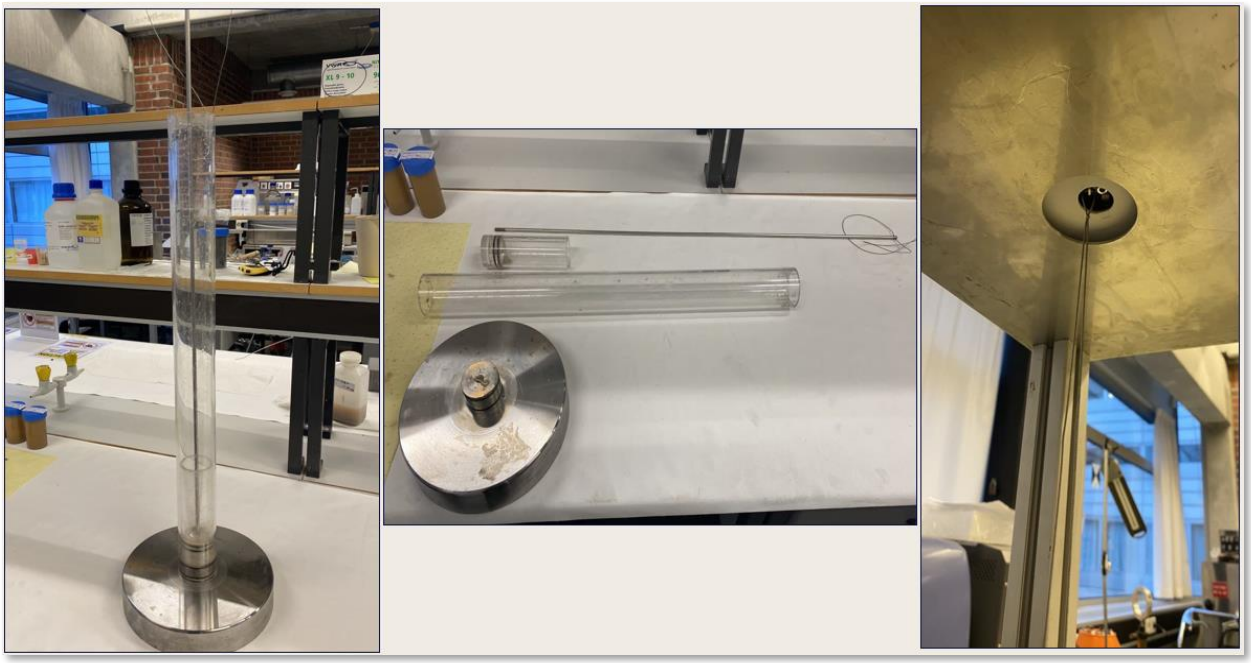

Figure 3- 1: Transparent pipe

It is open on top and sealed at the end without any leakage. A cup with 5 cm diameter and 10 cm length inside the pipe is held by a rod attached to scale.

3.1.2 Adventurer Balances (Lab Scale)

The Adventurer balance is a weighing instrument with high resolution. The OHAUS adventurer balances as shown in figure 3.2can measure the weight in the range of 120 gr to 8200 gr.

Figure 3- 2: Adventurer Balances OHAUS

Adventurer balance has different applications, and weighing is one of them. In this work, dynamic weighing was utilized since an unstable load was applied. The item, which is a cup in this investigation, was attached below the scale by rope, and the weight of the cup was measured over time and recorded by the Lab view program in PC.

3.1.3 Mechanical Properties Analyzer (MPRO)

MPro is an instrument that measures the elastic mechanical properties such as Poisson's ratio, young's modulus, bulk modulus) and compressive strength of API cement under high-temperature and high-pressure conditions. The equipment measures the compressional and shear sound velocities through the media, cementing and determining the Poisson's ratio and Young's modulus. MPro uses 5270 data acquisition and control system (DACS) and is furnished with a programmable temperature controller that measures temperature's impact on mechanical properties. There is an external Quizix pump system to provide realistic pressure and evaluate the impact on the mechanical properties. There are some benefits in MPro, such as mechanical properties measurement continuously. One single vessel provides sample

condition maintenance, and there is not needed separate procedure. This instrument is easy to install and use and has an optional external chiller system.

This equipment has a horizontal vessel. Since the Transducer and receiver are placed on the plugs sidely, and there is no risk of plugging the sides during the settlement leads to Signal interruption, the MPro is the appropriate equipment for indirect measurement of this experimental work. Quizix pump can provide the pressure which compresses the air bubbles in fluid affect on the particles settling.

Figure 3- 3: Mechanical properties analyzer

3.1.4 Hei-TORQUE 400 (Mixer)

Figure 3.4 shows the mixture utilized to make drilling fluid. The Hei-Torque 400 laboratory stirrer is suitable for liquid stirring with a viscosity of up to 250000 mPas or volume up to 100 liters (H2O). It is ideal to use up to 400 rpm for highly viscous media in the speed range that require mixing in a lower speed range. The maximum speed in operation can be 2000 rpm. There is the possibility of ramp programming, process monitoring such as timer function, torque trend display as a value, and the necessary equipment for documenting application parameters.

Figure 3- 4: Hei-TORQUE 400 (Mixer)

3.1.5 Hot roller (oven)

OFITE hot roller oven provides well condition for drilling fluid to study the temperature's effects on the fluid in circulation condition. The drilling fluid behavior will be monitored under pressure containers, and thermal effects in viscosity are demonstrated.

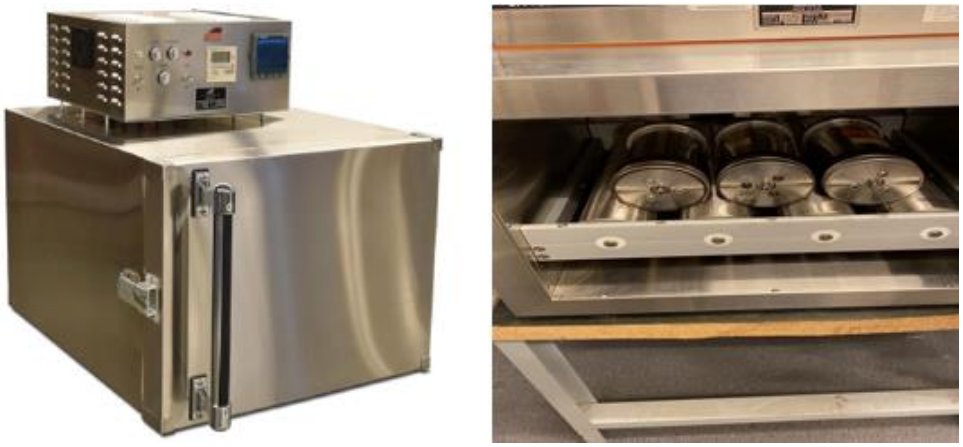

Figure 3- 5: High-temperature roller oven

The rolling speed in this oven is adjustable, and this oven is made of stainless steel to have a long life. There is a digital temperature controller to read the temperature from the outside of the oven. The samples can heat up in a range of 100 °F to 600 °F. one circulation fan is provided inside the oven, which improves air circulation. There are generally two modes in this equipment. In heating mode, it can be utilized for drying, aging, and baking in rolling mode. The oven can be used for making a homogeneous mixture of liquids and powders.

Thickening of some drilling fluids in downhole conditions with high pressure and high temperature is ordinary under static conditions and challenges drilling and completion operations. Aging tests are designed to predict fluid behavior in static and high-temperature conditions. In these tests, high-temperature aging cells are used. Figure 3.6 indicates a pressurized cell. In our study, these cells are utilized for hot rolling samples.

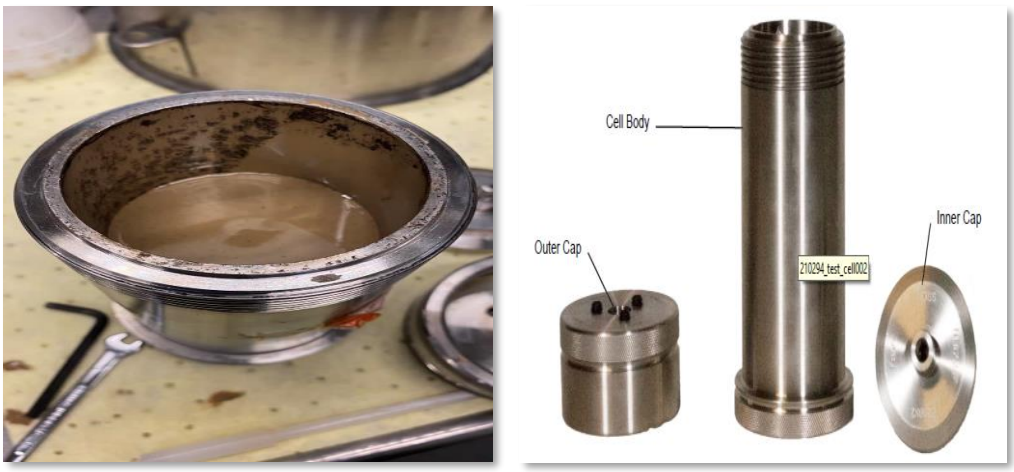

Figure 3- 6: High-temperature aging cell

3.1.6 Rotational Viscometer

This viscometer is an automated system that is designed for viscosity measurement. In this equipment, a coaxial cylinder rotational viscometer uses a spring. The spring measures the rotation angle of the bob inside the fluid sample. The annular space between the rotor and bob is filled by sample, and the bob is attached to a shaft with spring.

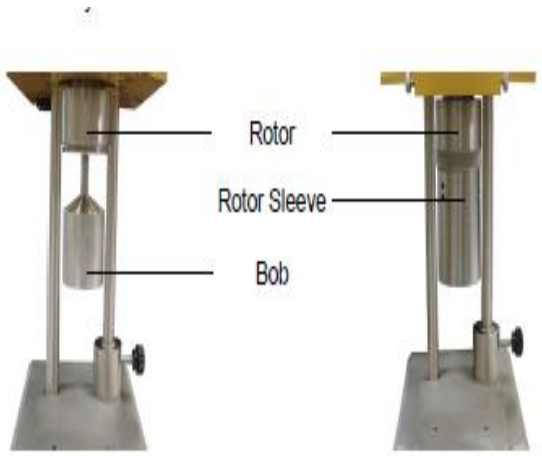

Figure 3- 7: OFITE model 900 viscometer

Fluid viscosity creates a torque on the bob and is monitored by the transducer, which measures the displacement of the bob. The main reason to use the rotational viscometer is quality check of the fluids by measuring their viscosity.

3.2 Mix designs

3.2.1 reference samples

The sample which is made to test includes barite, water, and xanthan gum (XG). Xanthan gum is a polysaccharide with high molecular weight, produced by the chemical breakdown of a substance by bacteria and other microorganisms. It is an effective stabilizer in a water-based fluid. XG has different utilization, ranging from the food industry to drilling fluid (Katzbauer, 1998). Barite has been described in detail in the first chapter. In this study, different recipes were suggested at the beginning of the experimental work. The difference between samples was the XG value. Four samples with different XG concentrations were made, as illustrated in Figure 3-1.

Table 3- 1: four different recipe for fluid sample

content	Fluid 1	Fluid 2	Fluid 3	Fluid 4
water	1000 ml	1000 ml	1000 ml	1000 ml
Micronized barite	156 gr	156 gr	156 gr	156 gr
Xanthan gum (XG)	0.6 gr	0.9 gr	1.2 gr	1.9 gr

Figure 3.8 indicates the sedimentation rate of samples that were measured and recorded after 24 hr settlement. Xanthan gum is a thickening agent and is very effective in increasing viscosity. It is necessary to mention that the sedimentation rate decreases as the XG value increases in the fluid.

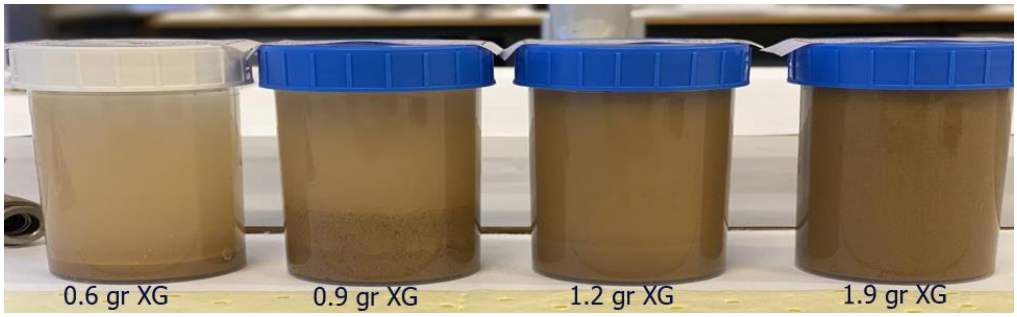

Figure 3- 8: samples settlement in with different XG concentration

Fluid with 1.2 gr XG is expected to sag with a clear transition fluid and barite within 24 hours, but as shown in Figure 3.8, there was no clear transition, and there was no transition in fluid with 1.9 gr XG. Then, except for two values, 0.6 and 1.2 gr XG, another value such as 0.9 was chosen to get reliable results.

3.2.2 Real samples

The system was calibrated by reference test, then two real samples regarding oil-based and water-based were suggested to prepare which used in the same tests. Tables 3-2 and 3-3 present the different recipes for water and oil-based mud.

Table 3- 2: OBM ingredients

Compound	Concentration by weight (gr)
Water	75
$Cacl_2$ solution	16.6
$Ca(OH)_2$	2
Emulator(primary and secondary) One-Mul	11.9
Mineral oil (EDC95/11)	174
Organic clay (versa vert vis)	8
Micronized Barite	138

Table 3- 3: WBM ingredients

Compound	Concentration by weight (gr)
Water	340
KCl	40
Soda ash (Na_2CO_3)	0.52
PAC LV	3
Starch	1.75
Xanthan gum	1
Micronized Barite	127

3.3 Experimental Methods

3.3.1 Drilling fluid preparing and mixing procedure:

The steps to prepare the reference samples are given:

1. 1000 ml of tap water is measured in the cup, which is used for mixing.
2. Measure the correct values of XG for different recipes
3. Pour the XG gradually and mix with low rotation 550 rpm
4. Mix for 10 minutes
5. Stacking up 156 gr of barite regarding the recipe6. Increase the mixing speed to 750 rpm and pour the barite gradually
7. Mix for 15 minutes

It is necessary to mention that the speed and mixing time was estimated based on the initial experimental tests conducted to get the ideal sample. Low-speed mixing for xanthan prevents breaking the gel strength. Based on the XG value used for preparing the sample, if a low value is consumed, we will have low fluid viscosity and high settlement rate, and we have to mix the barite with high speed and prohibit the sedimentation while mixing. Lower rotation can be used for high viscous fluid made by the high value of XG. The fluid should be mixed in the final step until the fluid sample lines disappear, as shown in Figure 3.10.

Figure 3- 9: Barite and XG measurement

Figure 3- 10: Fluid mixing

The procedure for making the real samples is defined as:

For oil-based mud:

1. Measure 75 gr tap water in the mixing cup.
2. Mixing 16.6 gr $Cacl_2$ with water in 5 minutes.
3. 2 gr Ca (OH_2) is added and mixed for 5 min.
4. Measure 11.9 gr one-Mule and add to the mixture with 10 min mixing.
5. 174 gr mineral oil is added and mixed for 10 minutes.
6. Mixing gradually 8 gr organic clay and then 5 minutes mixing

7. Pour 138 barite gradually and let the mixture under 25 minutes of mixing.

And for water-based mud:

1. 40 gr KCl is poured into the cup and mixed 5 minutes in 340 gr water.
2. Adding gradually 0.52 gr soda ash with 5 minutes mixing.
3. 3 gr of PACLV is combined with simple in 10 min.
4. Measuring 1.75 gr starch and add to mixture gradually, then let to mix 10 min.
5. 1 gr XG is measured and poured into the sample.
6. Finally, barite is mixed in concentration by 127 gr, and the sample is ready after 25 min mixing.

3.4 Test procedure

3.4.1 Transparent pipe test

The test was conducted at ambient pressure and temperature. The cup inside the pipe should be centralized and wholly suspended to have a good movement. As demonstrated in a schematic in Figure 3.11, the cup is attached to scale by a rope. The scale should be balanced on the structure. Then, the transparent pipe is filled with the fluid sample.

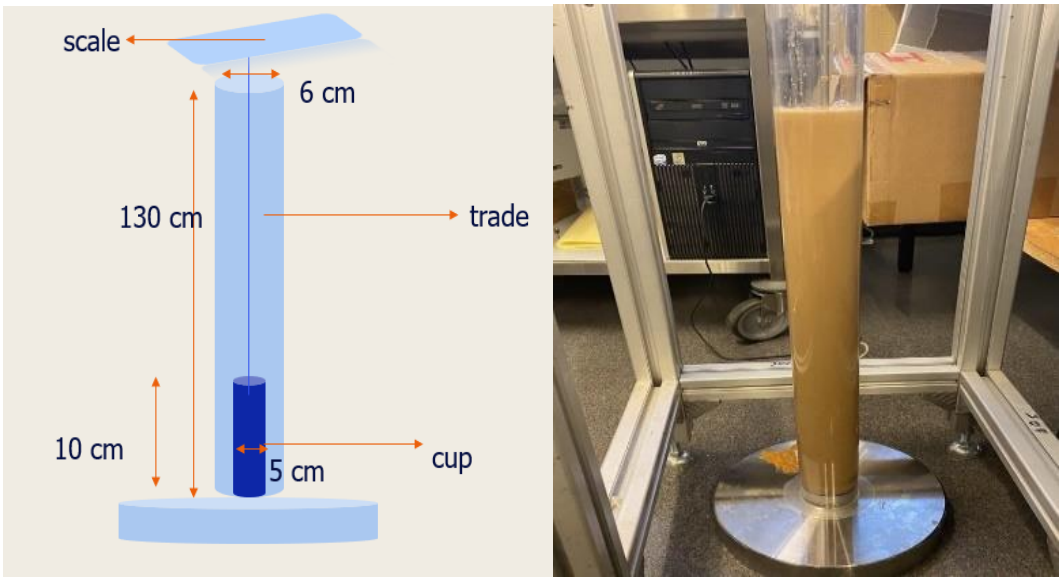

Figure 3- 11: transparent pipe schematic

The LabVIEW software is used to record the weight over time, and it is linked to the scale. Before running the LabVIEW, the scale should be tare to measure the net settled weight. Then LabVIEW can be started, and weight is measured. In those samples with low XG and high sag

rate, the time record can be adjusted every second to record the first phase of settlement more accurately, which has a dramatically increasing slope as indicated in Figure 3.12. For samples with high viscosity and low sedimentation rate due to the high-value xanthan consumed, the logging frequency can be every 5 seconds or higher. To get a reliable result, it is better to take a minimum of 24 hr test.

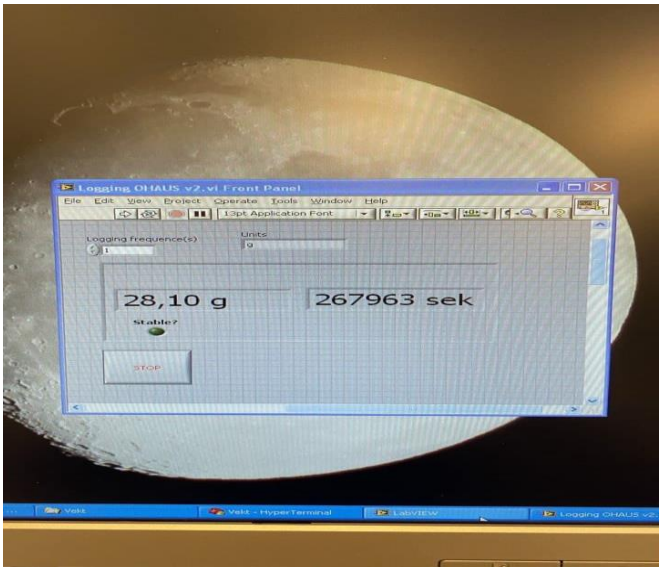

Figure 3- 12: lab view loggin

3.4.2 MPRO test

The pressure used in this test was chosen 1000 psi at ambient temperature.

The approach on how to test the samples in the MPRO is given below:

1. Remove the top and bottom plugs from the vessel
2. The inner tapered surface of the vessel should be greased by lithium Figure 3.13.

Figure 3- 13: Vessel inner surface Greasing

3. The center transducer element on the plug should NOT be greased.
4. Check the ports to verify that the pressure passages are not blocked.
5. Put the vessel on the table and hang it for filling with the sample.
6. Fill the vessel with fluid until the limit, which is defined by a gauge under the dry zone (Figure 3.14).

Figure 3- 14: filling level gauge

7. Insert the top and bottom plug into the vessel and hand-tighten.
8. Assemble the high-pressure gauge into the left port and thermocouple in the top plug.
9. Put the vessel in the heating and cooling jacket on the MPRO.
10. Connect the U_tube between the ports.
11. Connect the signal cables to the top and bottom connectors and vessels (Figure 3.15).

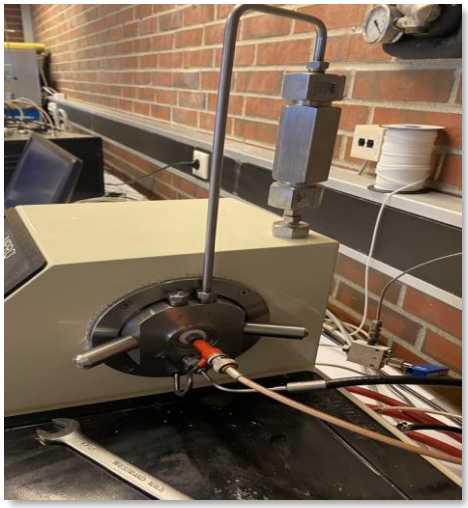

Figure 3- 15: Signal cables and connectors

12. Apply the pressure by pump works software on the pc:

- The pressure is applied to the vessel by two pumps connected to the MPro and make pressure by water injection and squeeze the air in the vessel. The pressure is applied gradually up to 1000 psi, as is indicated in fig Figure 3.16.
-

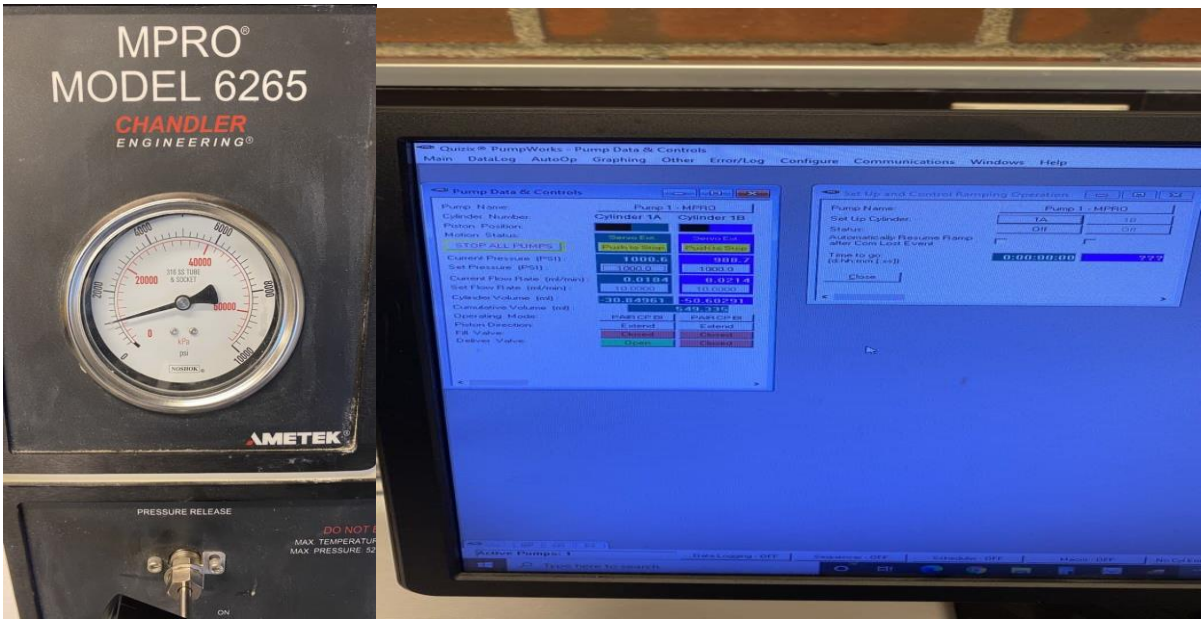

Figure 3- 16: pressure applied to the system

13. Run the 5270 DACS software, which is used with the MPro.

After running the test, transit time, shear time, temperature, and pressure are recorded continuously over time and logged as demonstrated in Figure 3.17.

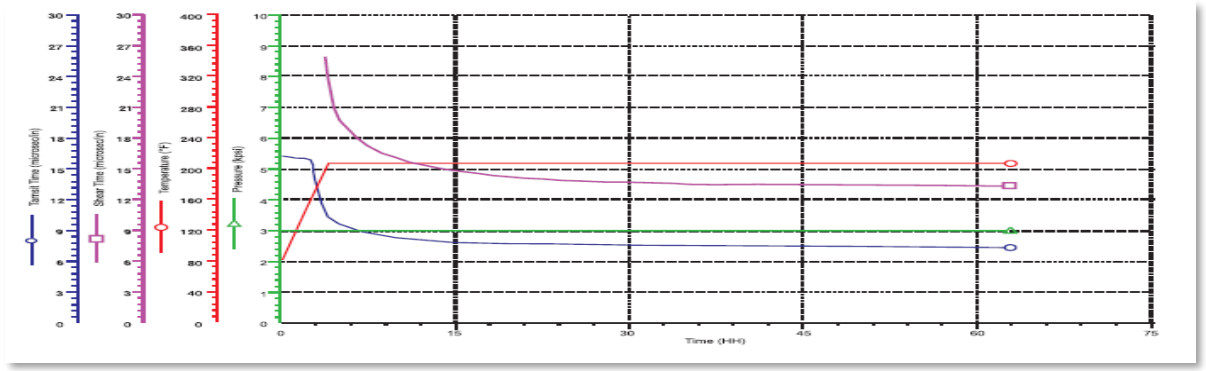

Figure 3- 17: Result logged from the mechanical properties analyzer(Arrow, 2015)

3.4.3 Rheology measurement

1. pour about 170 ml water into the cup.
2. After making sure that the bob is not in fluid, press the enter button and let the device be calibrated.
3. Lift the cup and put the bob in the fluid so that the fluid surface is placed between 2 holes on the bob, as shown in Figure 3.18.
4. There are numbered buttons on the right side which can be used for different shear rate.
5. Start with 600 rpm shear rate and read the displayed measurement, such as shear stress, shear rate, and viscosity.

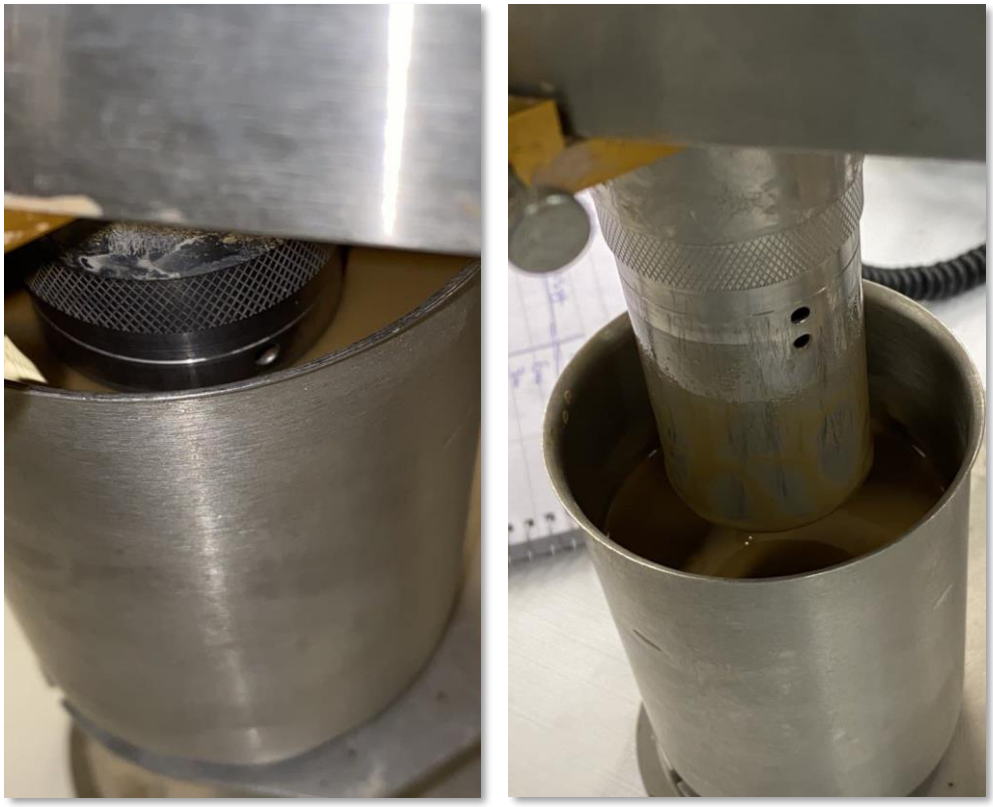

Figure 3- 18: cup capacity

By drawing the shear stress-shear rate curve, fluid flow behavior can be classified. Since drilling fluid contains particles longer than molecules, Newtonian's law does not apply for these types of fluid and is classified in non_Newtonian fluids depending on the fluid's composition.

3.4.4 Hot rolling

1. After making sure that the oven is connected to power, set the designed temperature.
2. Turn the heater on
3. The circulation fan will turn on when the heat switch is on. since fan blades are dangerous, turn the heater off when putting in or out the cells.
4. Pour the sample into cells. It is necessary to mention that the volume should not be more than 75% of capacity.
5. Make sure the cell's top plug is completely tightened.
6. Put the cells in the oven and turn the motor on to start rotation.
7. Use gloves to prevent injury.

Figure 3- 19 : Hot rolling

4. Result and discussion

In this chapter, a summary of the results will be given and discussed. A large number of samples are tested in this experimental work. The samples were categorized into reference samples and real samples references. Reference samples are investigated in different xanthan gum content. Water-based mud and oil-based mud are prepared as real samples. After getting the results from the transparent pipe test and mechanical properties analyzer in the direct measurement method, they are correlated with indirect measurements.

4.1 System modification

The initial results from the reference sample showed high fluctuation in barite settled weight over time. It was discovered that there was some uncertainty such as buoyancy effect, which affected barite weight in the cup. Decreasing the measured weight of settled barite in the cup indicated that some of the barite particles were settled on the edge of the cup. There was also a small space between the cup and bottom of the pipe, which was filled quickly by the particles that pass through of annular space between the cup and pipe and settled on the bottom of the pipe.

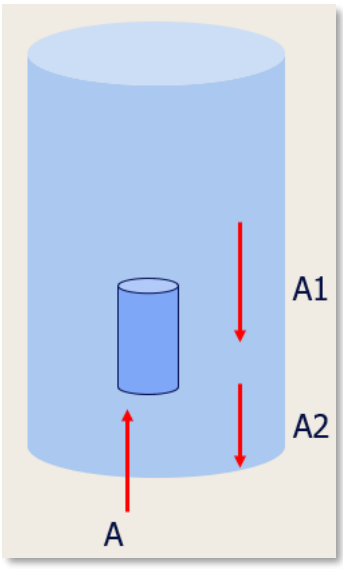

Figure 4- 1: buoyancy effect

As Fig 4.1 illustrates, two factors can have a negative effect on buoyancy force.

A1 = due to increasing the deposit weight

A2 = decreasing the fluid density during the settlement

BF (buoyancy effect) = A -A1-A2

If the buoyancy factor is high, the measured weight of the cup does not show the whole weight of the settled particle correctly due to the buoyancy effect. To compensate for the buoyancy effect, it is decided to make the cup material with metal to make it heavier and sharpen the edge of the cup on both sides. The sharpness of the edge was decided to prevent settling on the wall thickness.

The rope which hangs the cup inside the pipe was cut to 28 cm. sharpness on the bottom side of the cup decreased the buoyancy factor due to the less surface area.

4.2 Rheology measurement

Rheology measurement for three recipes with different XG values is demonstrated in Figure 4.2. As it is indicated, shear stress shifted up due to the XG increasing. In the sample with high XG, shear stress is higher than other fluid types. Due to the more substantial network structure resulting from polymer entanglements, sample with higher XG volume has more susceptibility to keep the particle against the settlement.

Table 4- 1 : shear stress-shear rate values for reference sample

shear rate (1/s)	0.6 gr XG shear stress (lb/100 ft^2)	0.9 gr XG shear stress (lb/100 ft^2)	1.2 gr XG shear stress (lb/100 ft^2)
1021.38	10.3	12.9	15.1
510.69	6.6	7.4	10
340.46	4.8	5.4	7.8
170.23	2.9	3.5	4.8
102.14	1.7	2.6	3.8
51.07	1.2	1.6	2.6
34.05	1.1	1.3	2.2
17.02	NA	NA	NA
10.21	NA	NA	NA
5.11	NA	NA	NA
3.4	NA	NA	NA
1.7	NA	NA	NA

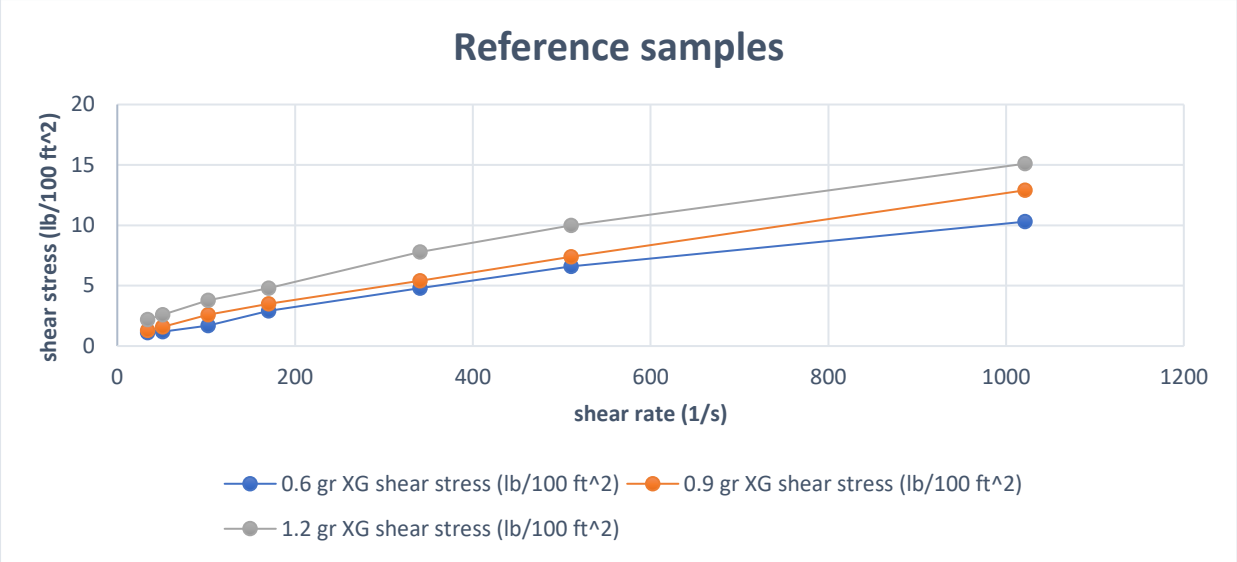

Figure 4- 2: shear stress-shear rate for references samples

It is necessary to mention that shear stress values are valid for a high shear rate. Since the viscosity is very low in a low shear rate, the bob in the viscometer cannot measure the shear stress. Then the values can be the same in low shear rate and are not reliable.

Figure 4.3 shows the shear stress-shear rate measurement for water-based mud before hot rolling and after hot rolling. It is evident that viscosity decreased after hot rolling. As shown in Figure 4.3, the yield stress of water-based mud increased due to the hot rolling. In our test, when we pour the sample, we are near to the zero shear rate.

Table 4- 2: shear stress-shear rate values for water-based mud

shear rate (1/s)	**shear stress (lb/100 ft^2) before hotrolling**	**shear stress (lb/100 ft^2) after hotrolling**
1021.38	56.1	44
510.69	35.9	31.3
340.46	27.6	25.2
170.23	17.4	17.9
102.14	11.4	14.1
51.07	7.6	10.5
34.05	6.2	9.2
17.02	4.5	7.3
10.21	3.4	6.1
5.11	2.7	5
3.4	2.5	4.7
1.7	2.1	4

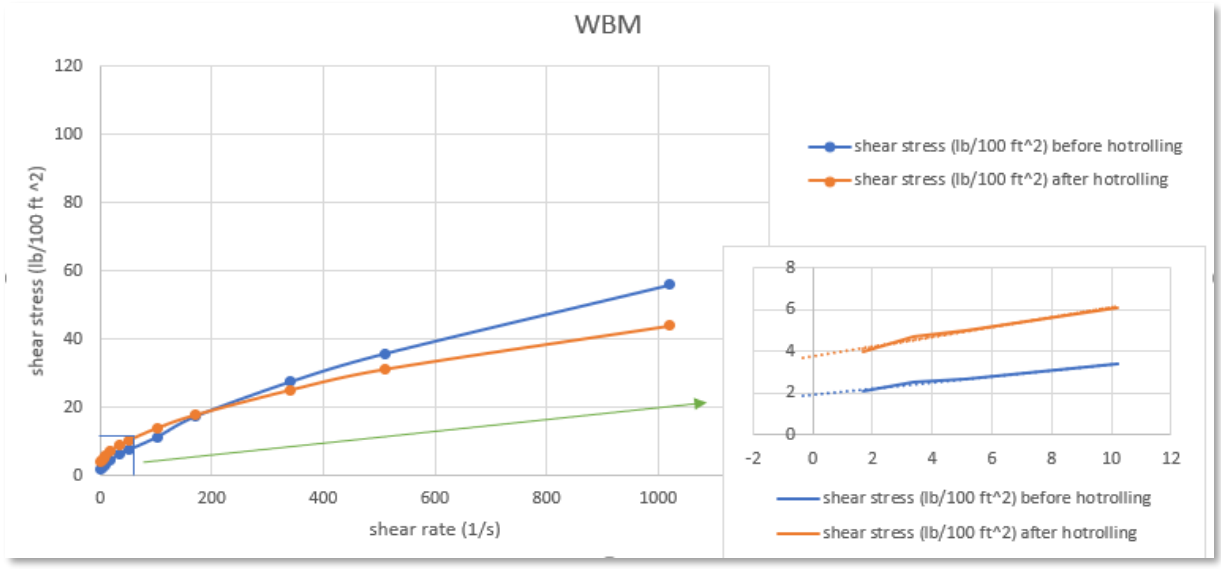

Figure 4- 3: shear stress-shear rate for water-based mud

Shear stress over the shear rate for oil-based mud sample recorded and indicated in Figure 4.4. It is revealed that viscosity increased after hot rolling, and yield stress also increases due to the hot rolling. As it is seen, shear stress at zero shear rate increased from 1.8 lb/100 ft^2 to 2.9 lb/100 ft^2.

Table 4- 3: shear stress-shear rate values for oil-based mud

shear rate (1/s)	shear stress (lb/100 ft^2) after hot-rolling	shear stress (lb/100 ft^2) before hot-rolling
1021.38	101	81.7
510.69	59.8	49.1
340.46	43	34.7
170.23	25	19.4
102.14	17.1	12.9
51.07	11	7.8
34.05	7.6	5.2
17.02	5.4	3.7
10.21	4.3	3.2
5.11	3.6	2.3
3.4	3.4	2.1
1.7	2.9	1.8

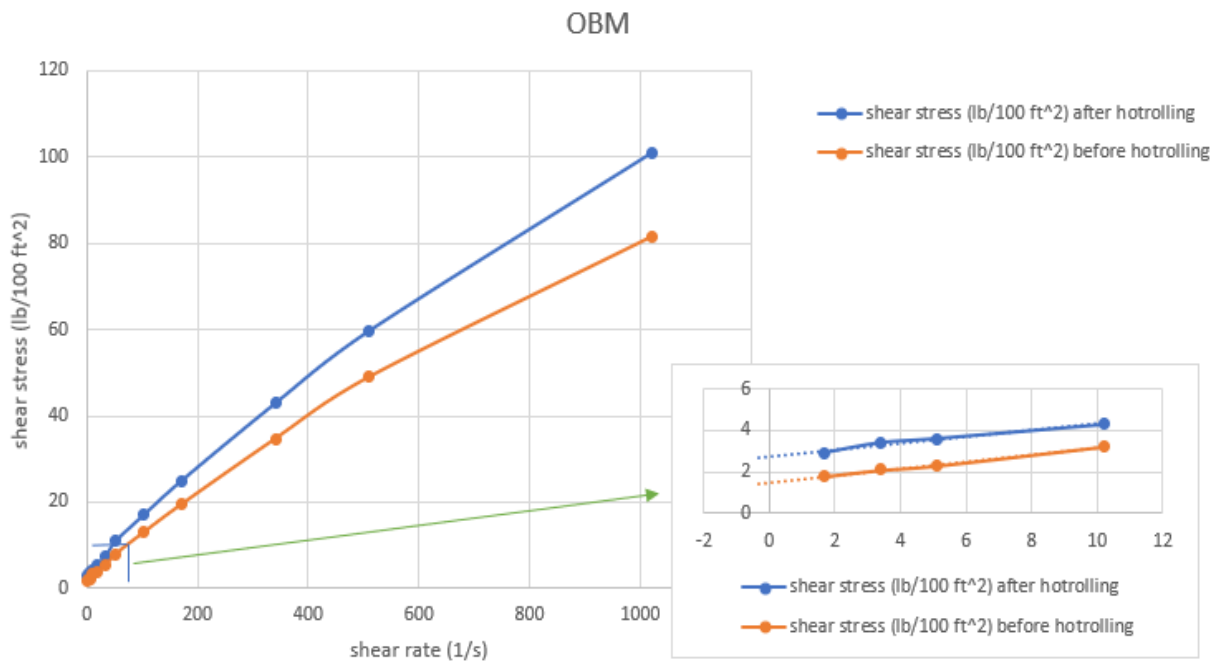

Figure 4- 4: shear stress-shear rate for oil-based mud

4.3 Reference samples

The first tests were conducted in the transparent pipe using the reference samples two times for each XG content with the same barite to investigate how the XG content affects the sedimentation rate. The samples were prepared using 0.6, 0.9, and 1.2 gr XG. As figure 4.5 indicates, the weight of settled barite increases over time. The settling is high in the first hour for all cases. In the sample with 0.6 XG, the weight of settled barite reached approximately 53 gr, and then it increased gradually and reached 75 gr after 8 hrs and got constancy. With increasing the XG value to 0.9 gr in the sample, the sedimentation rate decreased so that In the first hour, about 51 gr barite settled and will be constant, which means there is no settlement during the rest of the test. Regarding the case that includes 1.2 gr XG, the scale recorded about 12 gr barite settlement in the first hour, and it gradually grew to 25 gr after 22 hrs.

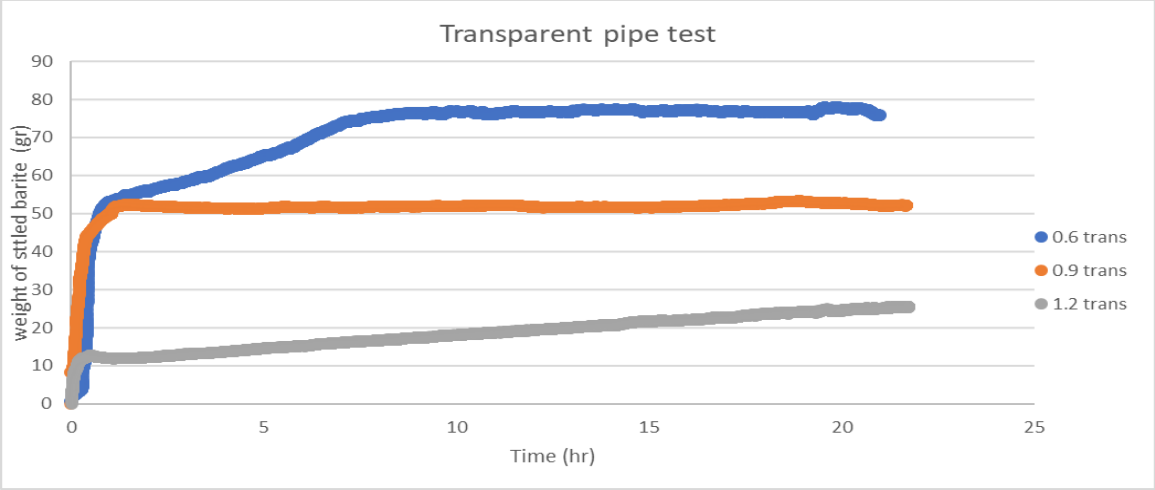

Figure 4- 5: Transparent pipe test for reference samples

The result confirmed the fact that those samples that included more XG value have less sedimentation rate. Since XG is a viscosifier and a strong stabilizer, it takes a long time to settle the whole of barite particles, and XG keeps the particle in suspension. The sedimentation rate increased and more barite settled in the case in which less XG was employed. This proves the system's consistency in measurement.

In direct measurement, as demonstrated in figure 4.6, since there is long vertical distance in transparent pipe for particles settling, hindered effect is dominant and measured in this method.

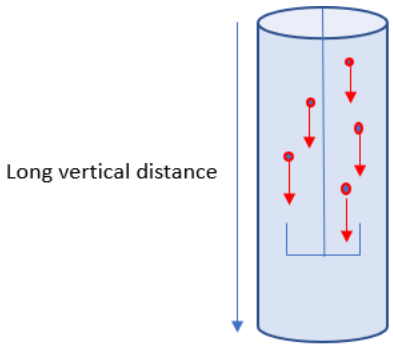

Figure 4- 6: Direct measurement (Hindered effect)

Figures 4.7, 4.8, and 4.9 display the settlement procedure in 3 different times for 0.6, 0.9, and 1.2 gr XG. As seen, the clarification zone for samples with a mean of 0.6 and 0.9 gr XG is more obvious than a sample with 1.2 gr XG .

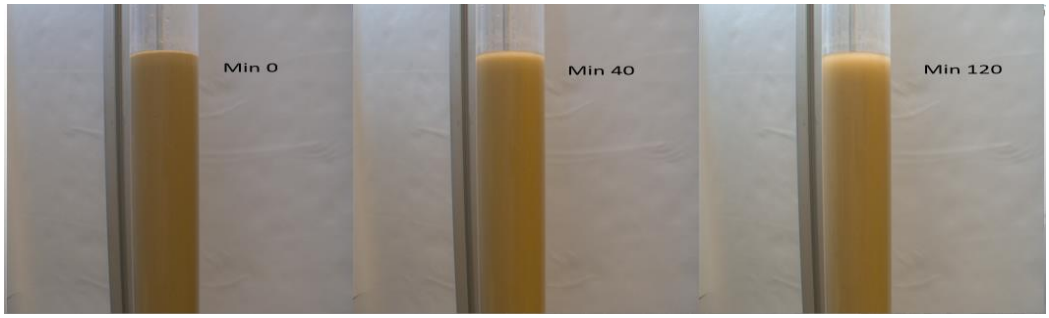

Figure 4- 7: Particle Settling schematic for 0.6 gr XG

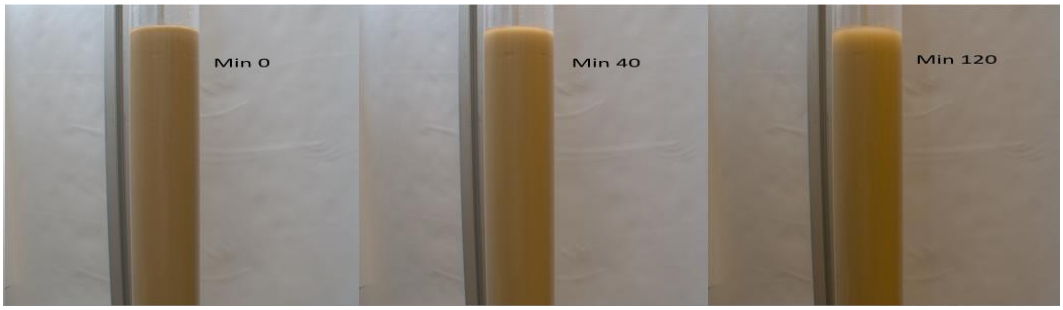

Figure 4- 8 : Particle Settling schematic for 0.9 gr XG

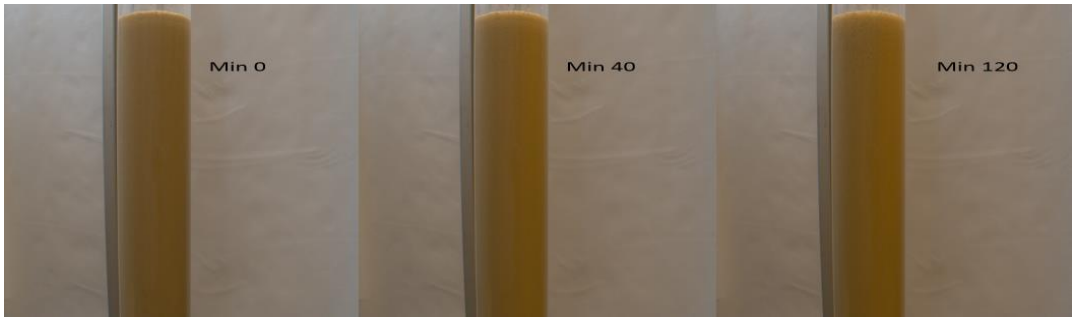

Figure 4- 9: Particle Settling schematic for 1.2 gr XG

As shown in figure 4.10, Vertical distance in vessel inside the Mpro is short compare to the transparent pipe . It takes short time to settle the particle on the lower side of vessel then boycott effect can be obvious and measured by indirect measurement.

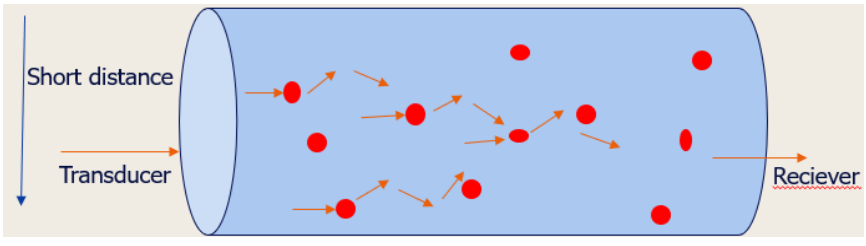

Figure 4- 10 Indirect measurement (Boycott effect)

Figure 4.11 demonstrates curve fitting in regression analysis using power model for different XG content. The appropriate correlation with R-square = 0.926 can be presented :

$$Y = 9.133\ x^{0.321} \qquad \text{Eq 18}$$

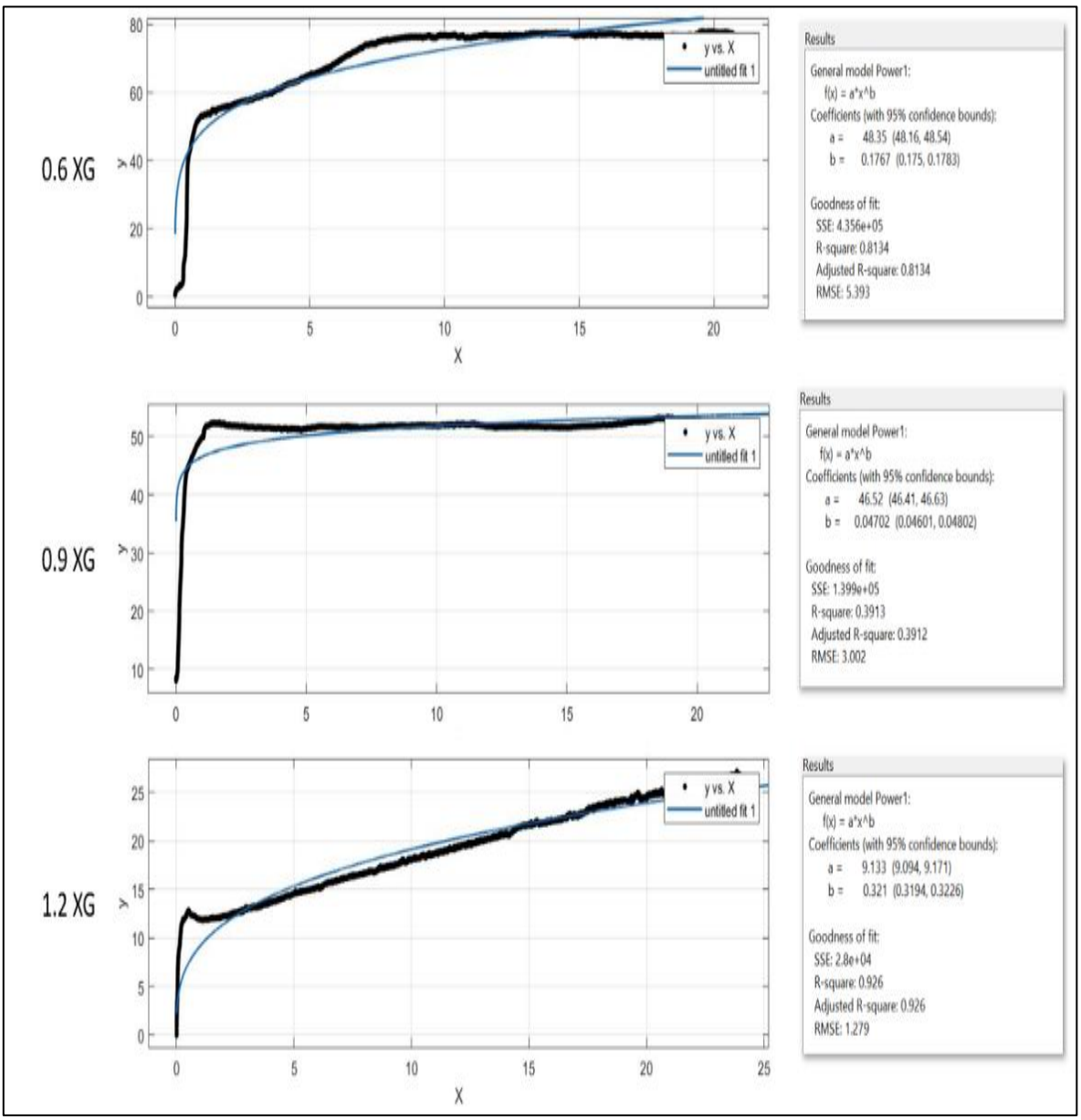

Figure 4- 11 : Regression analysis and curve fitting

Figure 4.12 indicated the result of the MPro test, which was run for reference sample over 24 hrs with 0.6 gr barite. Transit time decreased rapidly in the first hour from 34.58 microsec/in to 34 microsec/in, and then it reached 33.8 microsec/in.

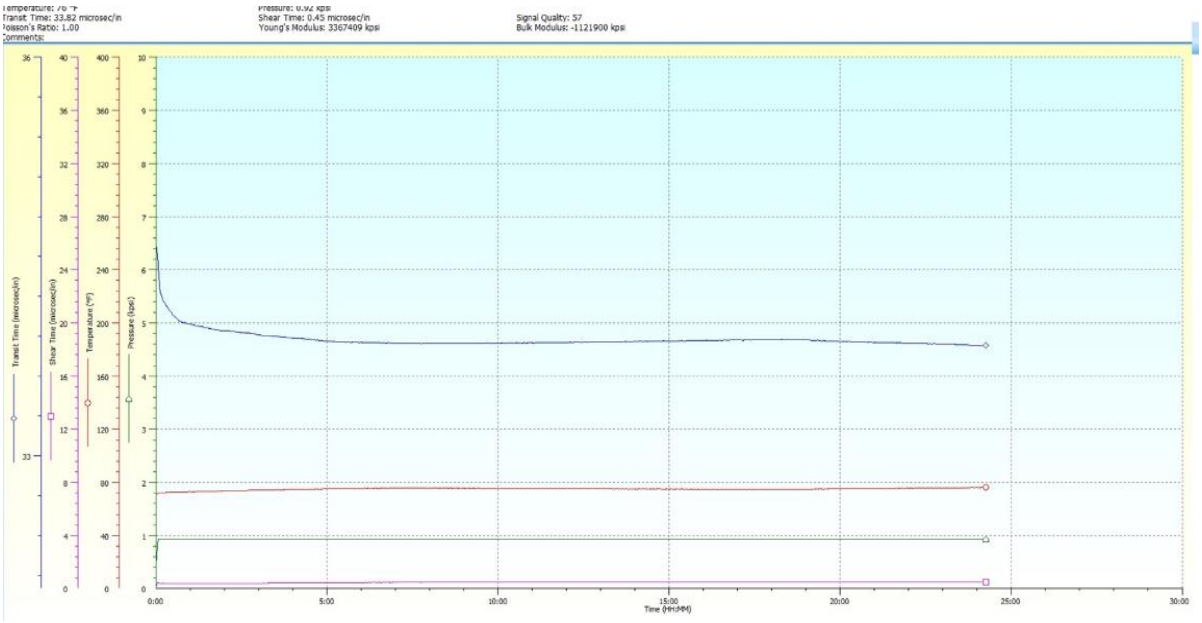

Figure 4- 12: MPro test for reference sample with 0.6 gr XG

If it is shown in high resolution like Figure 4.13, there is fluctuation after dropping. However, the whole trend is descending.

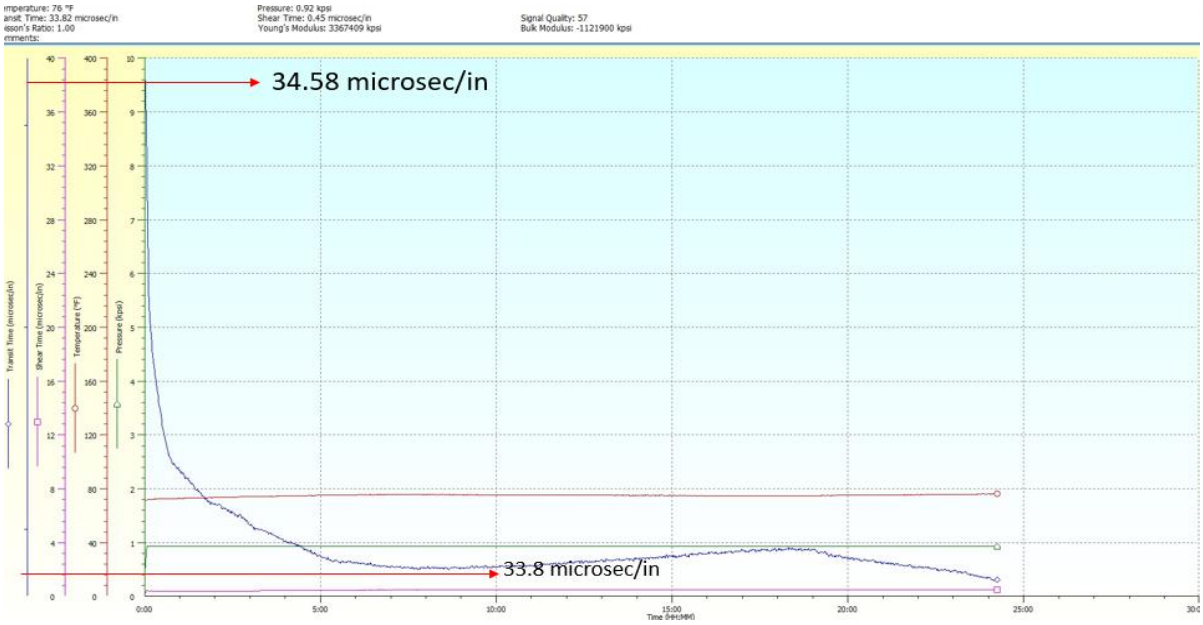

Figure 4- 13: MPro test result for 0.6 gr XG in high resolution

Since the mechanical properties analyzer measures compressional wave, vibration occurs when the wave hits the particles. Then it takes a longer time to pass from transducer to receiver through the vessel. As it is demonstrated in figure 4.14, There is less hitting to particle those

settles and the number of suspended particles decrease. The compressional wave can pass the media without any collision, and it can be said that the transit time decreases.

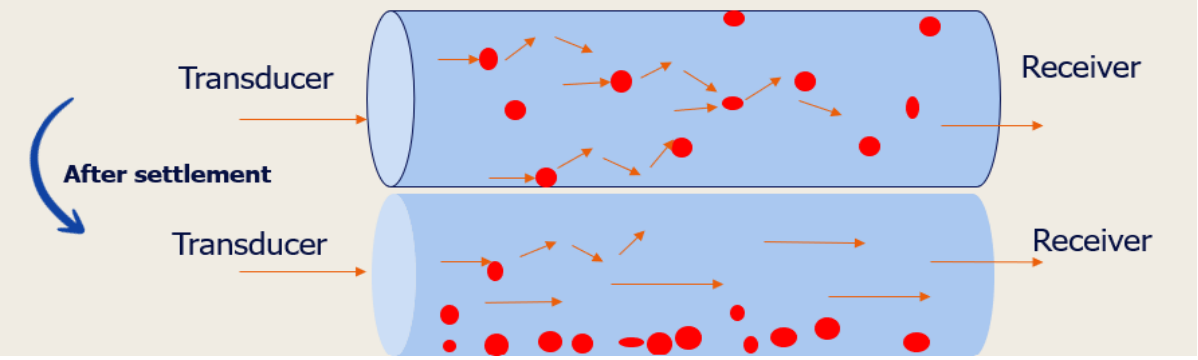

Figure 4- 14: Visionary drawing effect of the settlement on transit time.

Figure 4.15 demonstrates the comparison of settlement behavior in two different tests for the sample with 0.6 gr XG. It is clear that in both tests, in the first hour, there is a high sedimentation rate as it is indicated in the transparent pipe test by rapid weight increasing and sudden decreasing of transit time in MPro test, and the trend has been smooth at the rest of the tests.

The result revealed that during the settling, the transit time decrease due to the fewer suspended particles.

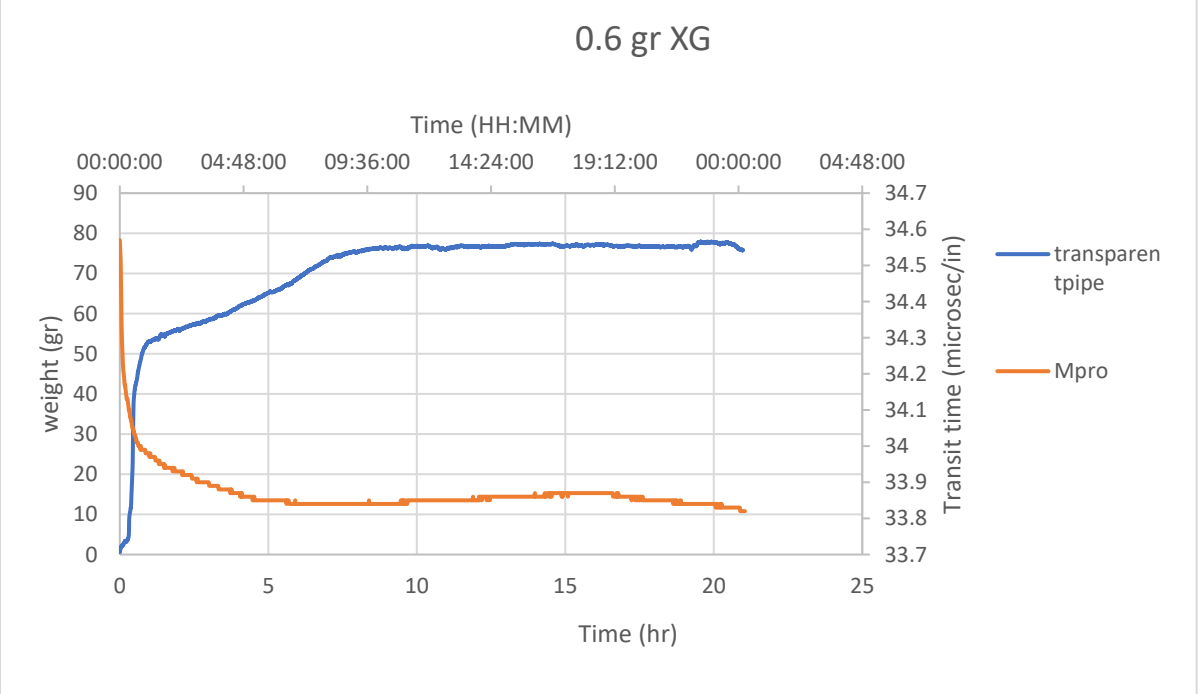

Figure 4- 15: Comparison of MPro test and transparent pipe test result for 0.6 gr X

As mentioned earlier, in direct measurement, hindered effect is noticeable, and the boycott effect is susceptible in indirect measurement. Regarding figure 4.15, the time parameter for direct measurement and indirect measurement does not necessarily match because the distance and settling time in direct and indirect measurement are different.

As indicated in Figure 4.16, MPro result for the sample with a 0.9 gr XG sample reveals that transit time has a steep decrease for the first hours. This steep is less for the first 5 hours compared to the sample with 0.6 gr XG. Transit time decrease from 34.3 microsec/in to 34.1 microsec/in after 7 hours. Then can be seen a smooth increase in transit time of about 0.1 microsec/in for 12 hours, and after 19 hours, the transit time starts to decrease again until it reaches 34 microsec/in at the end of the test.

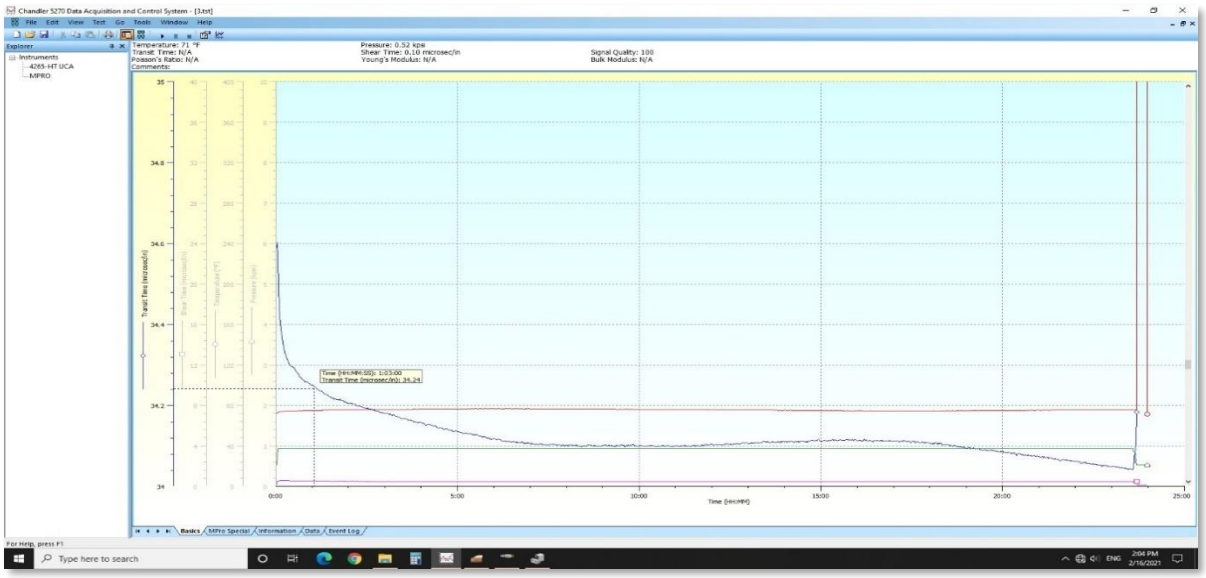

Figure 4- 16: MPro test result for reference sample with 0.9 gr XG

In Figure 4.17, decreasing the whole trend is observed.

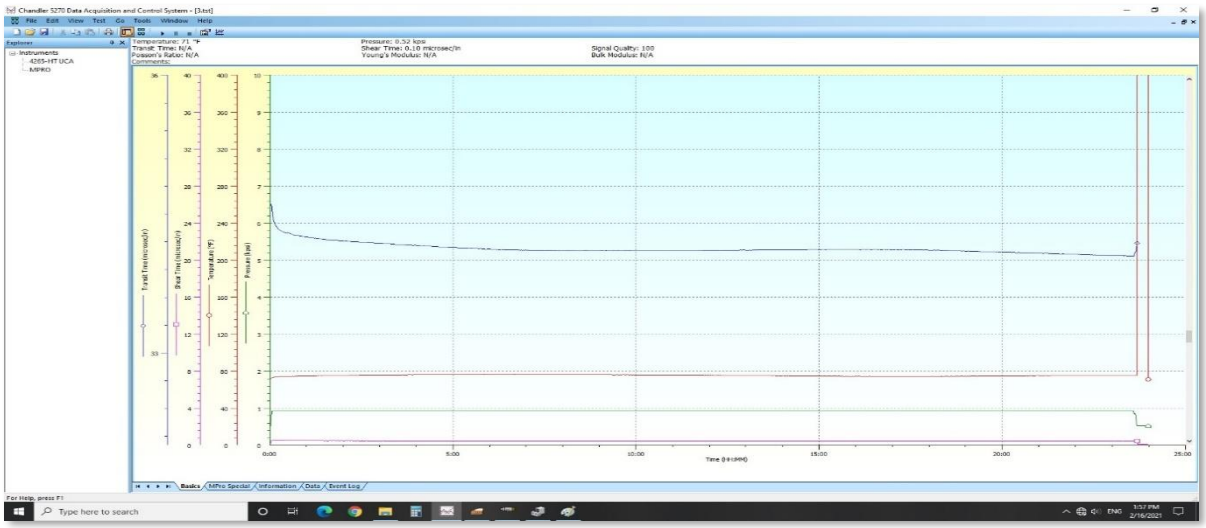

Figure 4- 17: MPro test result in low resolution for 0.9 gr XG smaple

Figure 4.18 demonstrates how the trend is opposite between MPro test result and the transparent pipe one. It revealed that the rate of settling is highest in the beginning, so that settled weight reaches about 50 gr. Meanwhile, transit time dramatically reduces, and then the sedimentation rate increases smoothly and continuously throughout the test period. The big particles started to settle in the first minutes of the test and led to significant sag weight increasing.

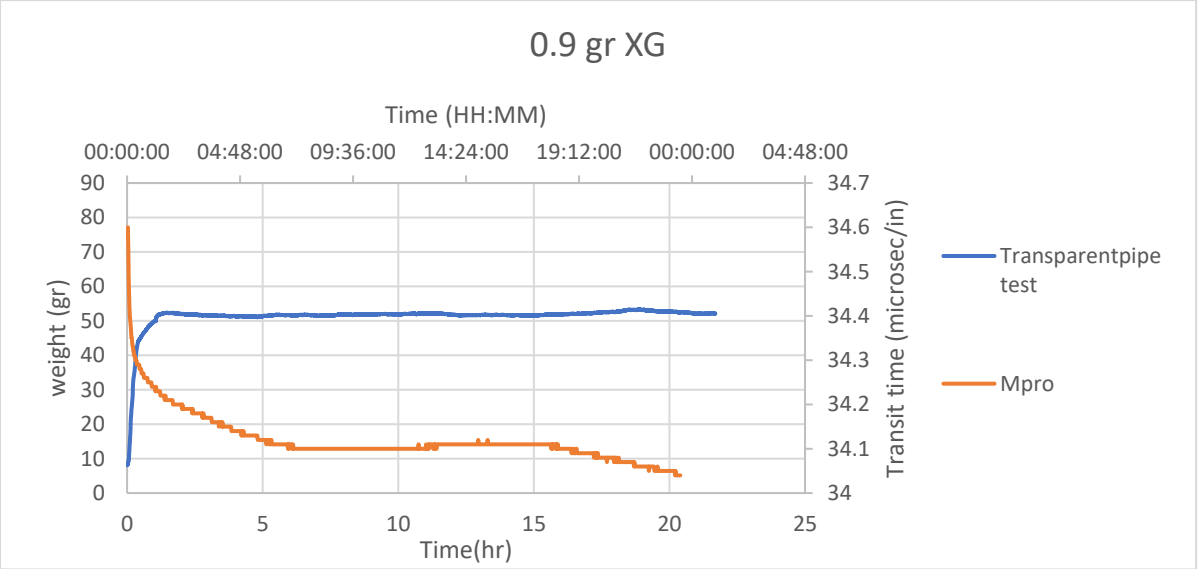

Figure 4- 18: comparison of MPro test and transparent pipe test result for 0.9 gr XG

Another MPro test done for the sample with 1.2 gr XG, is demonstrated in figure 4.19. As illustrated, transit time decreases dramatically from 34.47 microsec/in to 34.3 microsec/in in 30 minutes. Transit time starts to increase from 34.3 and reaches 34.34 micorsec/in before it increases slowly in the last hours.

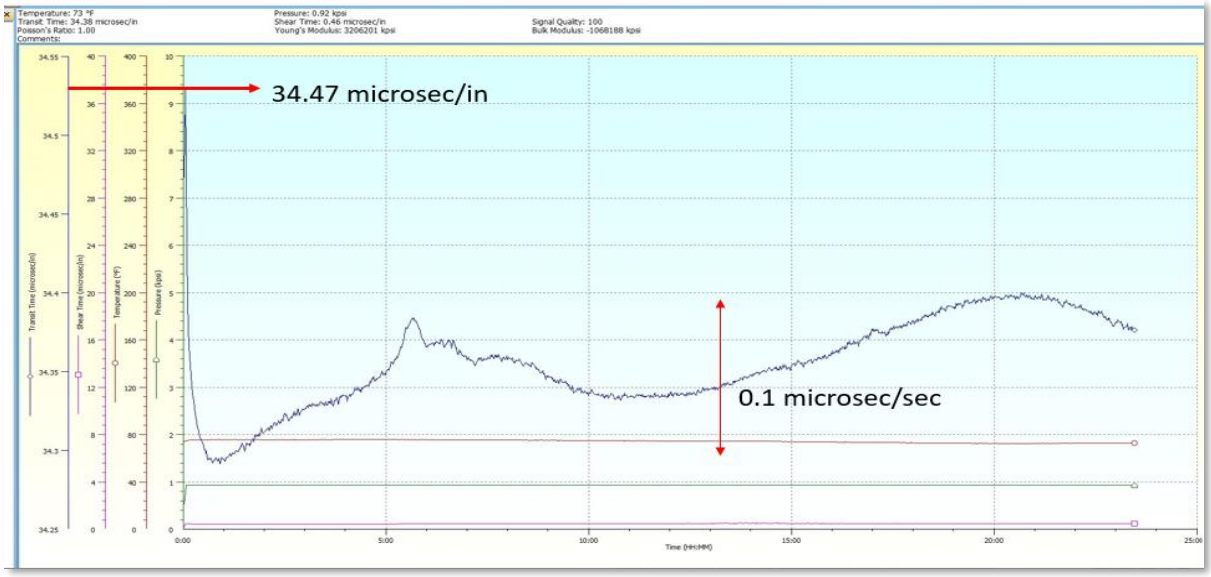

Figure 4- 19: MPro test result for reference sample with 1.2 gr XG

It can be seen there is just 0.1 microsec/in fluctuation, and the whole trend is decreasing, as it is shown in Figure 4.20, which displays the low resolution of the result.

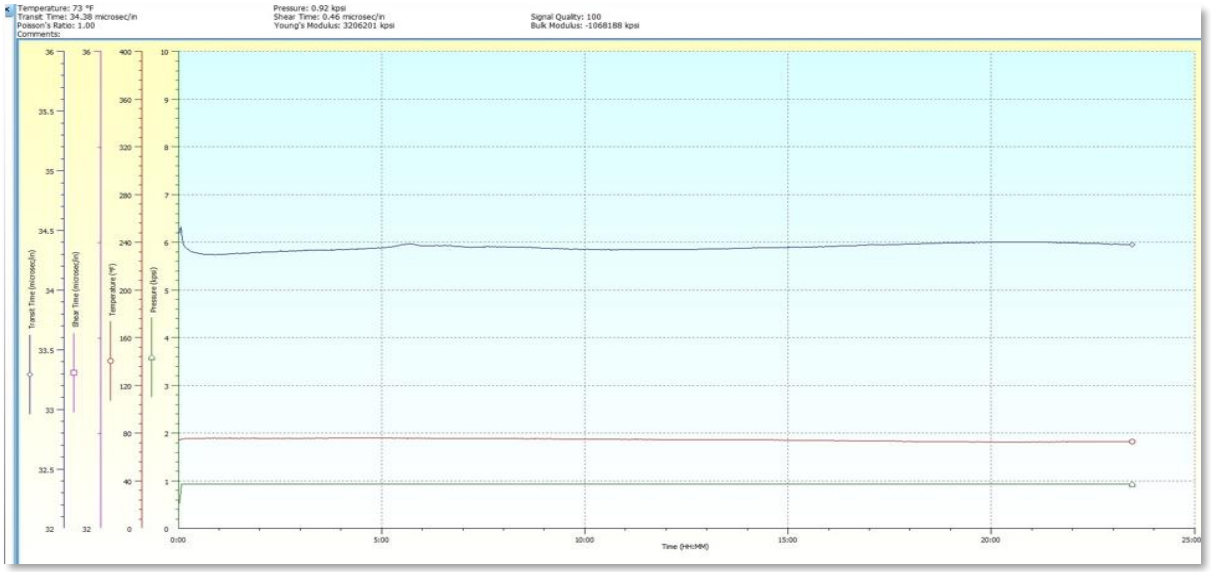

Figure 4- 20: MPro test result in low resolution for 1.2 gr XG sample

The comparison between MPro test result and the transparent pipe test result for the sample with 1.2 gr XG is indicated in Figure 4.21. It can be expected that there is a quick signal traveling through the media due to the significant separation tendency of large particles in the first minutes. In this time, the settled weight increased rapidly, and then the settling rate gradually increased by the rest of the particles so that the cup had approximately 27 gr settled barite at the end of the test. The result revealed that The fluid with high XG has more capability to keep the particles suspended due to the gel strength and the number of hefty particles that settled quickly at the first of the test is less compare to the other samples with lower XG value. The instability of the result at the rest of the test for MPro can be due to signal fluctuation.

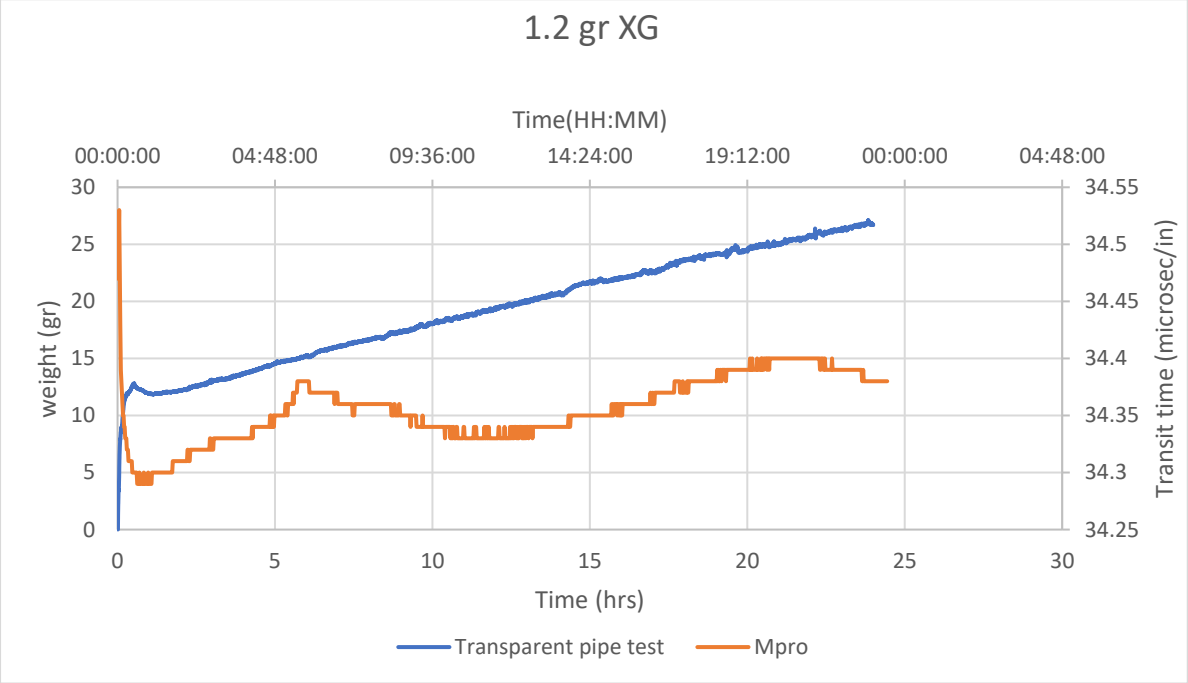

Figure 4- 21: comparison of MPro test and transparent pipe test result for 1.2 gr XG

4.4 Real samples

4.3.1 Water-based mud (WBM)

Figure 4.22 represents the results from different transparent pipe tests were conducted for water-based mud. The results indicate that the barite settled weight reached a range of approximately 17-25 gr in different experiments. Some decrease is evident at the first of the tests. The buoyancy effect can be dominant at the first of the tests, where there is not settled weight in the cup.

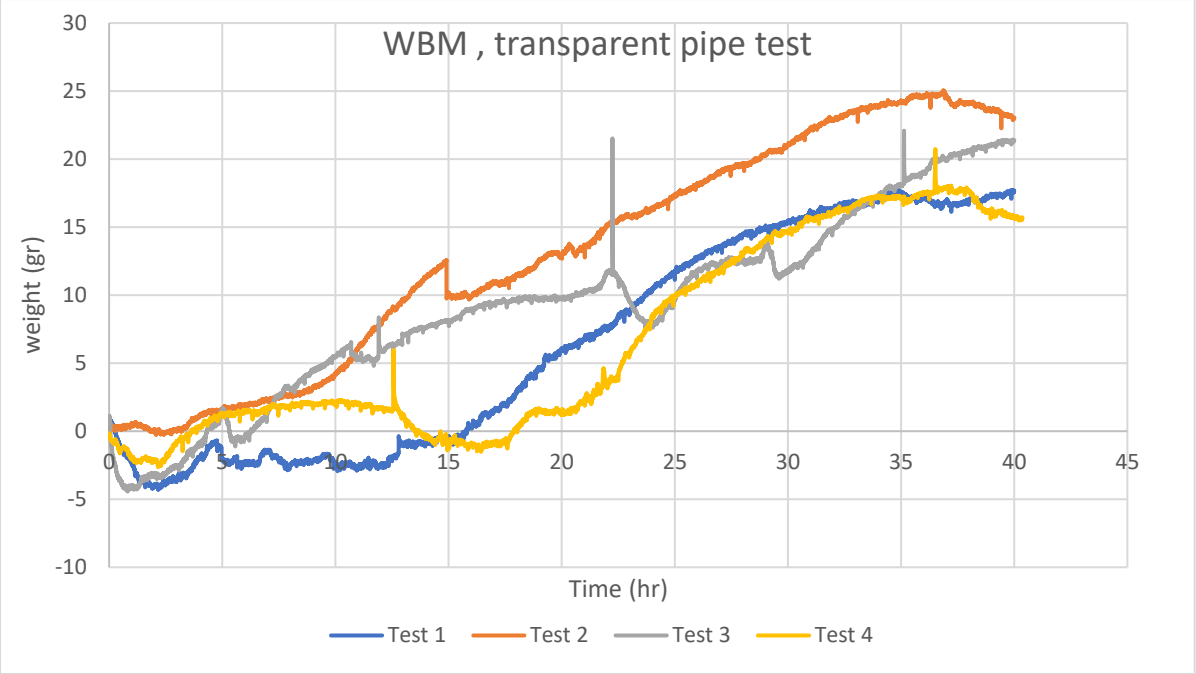

Figure 4- 22: Transparent pipe test results for water-based mud

In test number 2, a steep slope is evident for about 5 hours due to the friction. In this test, the trend after 15 hours followed the general slope and suddenly decreased to return the real weight. Mostly, the trends are the same, and the settlement rate started to increase and got faster after 15 hours.

To find a correlation based on direct measurement result for water-based mud, non-linear regression has been taken for all of the tests. Figure 4.23 shows the curve fitting for different test results.

Equation regarding test two with high R-Square (0.9731) can present an appropriate correlation for barite settling behavior over time in water based mud which is :

$$Y = 0.5239 \, x^{1.073} \qquad \text{Eq 19}$$

Regarding Eq 18 and Eq 19, water based mud and reference samples have different behavior in barite settling. Another correlation will be presented further for oil-based to get a comparison with other samples.

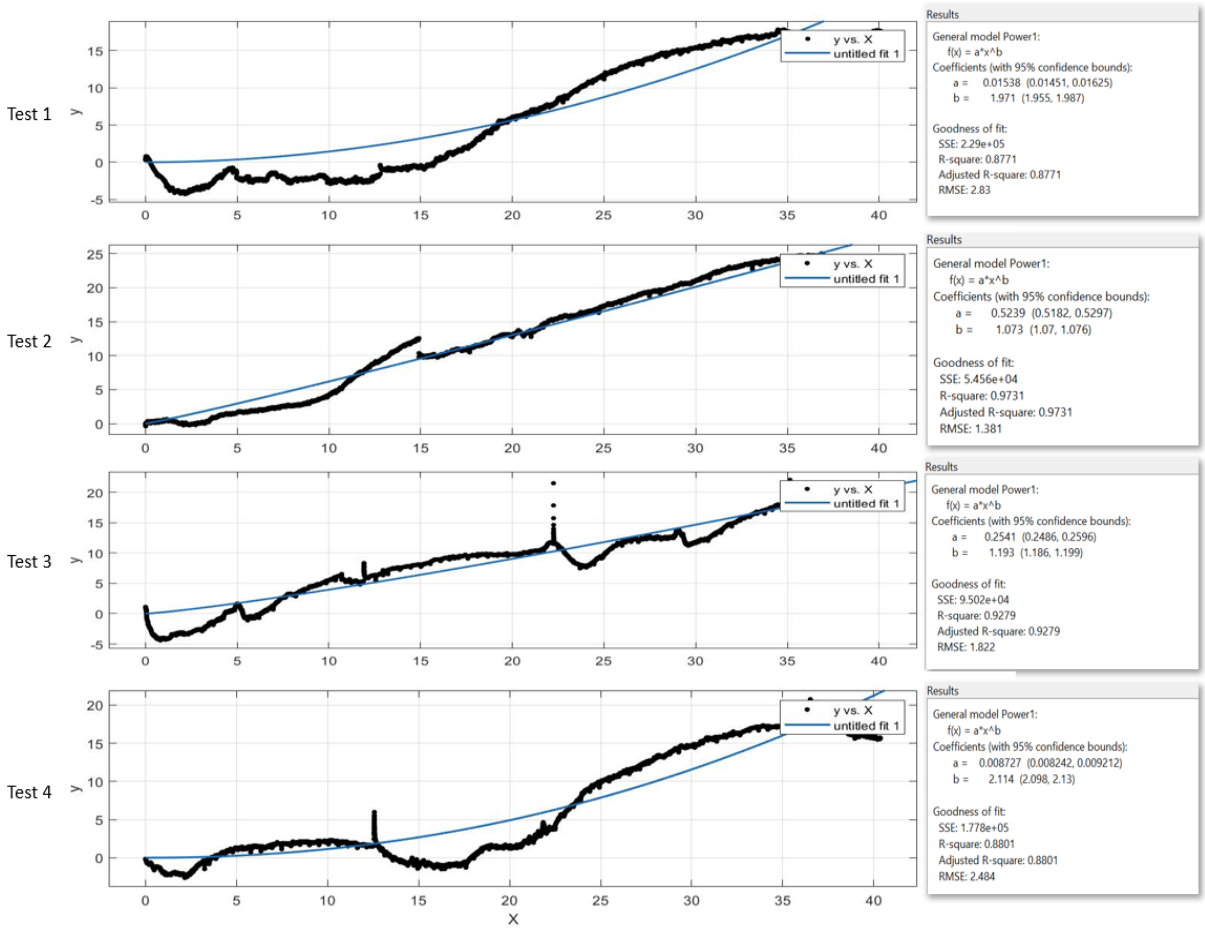

Figure 4- 23 : Regression analysis and curve fitting

The MPro test result for water-based mud is illustrated in figure 4.24 over 24 hours. As indicated, transit time decreased from 32.7 microsec/in to 32.6 after 7.5 hours and was almost constant for the next 7.5 hours. Then it had an increase to reach 32.66 microsec/in.

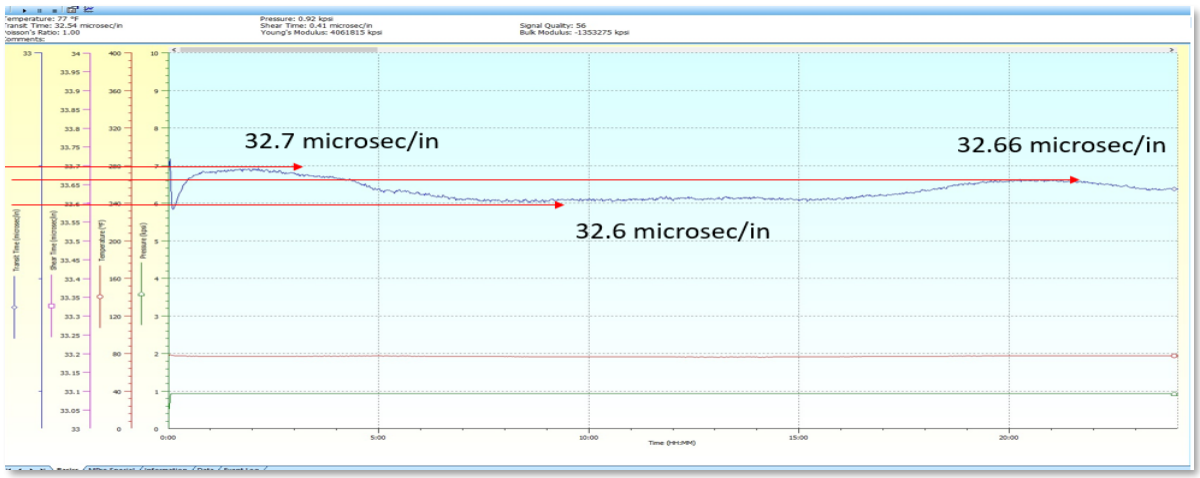

Figure 4- 24: MPro test result for water-based mud

Figure 4.25 demonstrates a comparison between settlement rate and transit time trend. As it is shown, as the barite particles started settling out of the suspension and sedimentation rate increased, the transit time decreased.

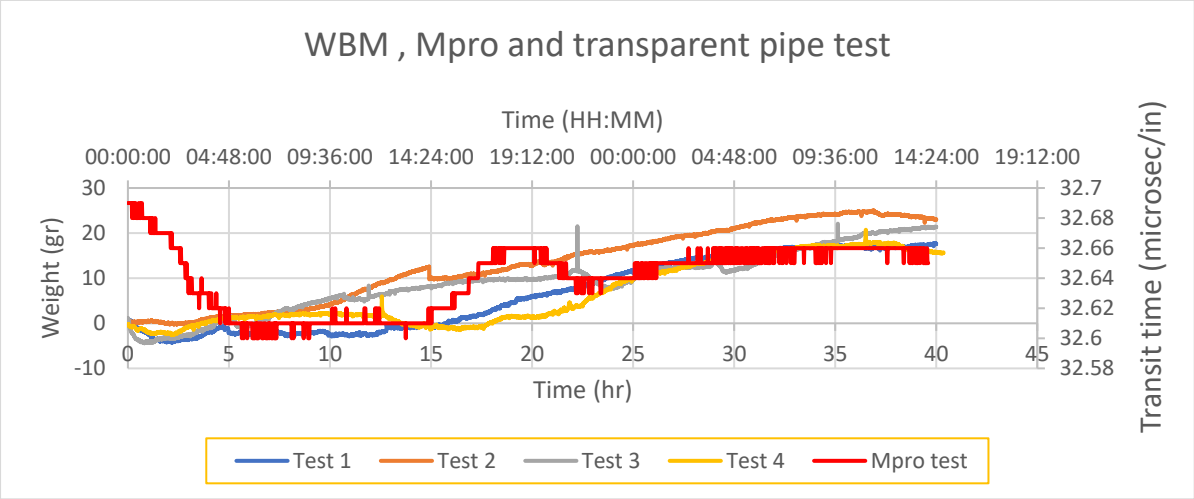

Figure 4- 25: MPro and transparent pipe test result comparison for water-based mud

4.3.2 Oil-based mud (OBM)

Other experiments were carried on using oil-based mud for the transparent pipe test. Fig 4.26 shows the result for three different tests were performed over 40 hours. In all the tests, the settling rate had a sharp increase in the first approximately 10 hours. The decreasing trend is observed for tests which can be due to the buoyancy effect and ambient temperature fluctuation. Then, the settled weight started to increase slowly after 26 hours and continued throughout the test period. Finally, the barite settled reached the range of 8-11 gr.

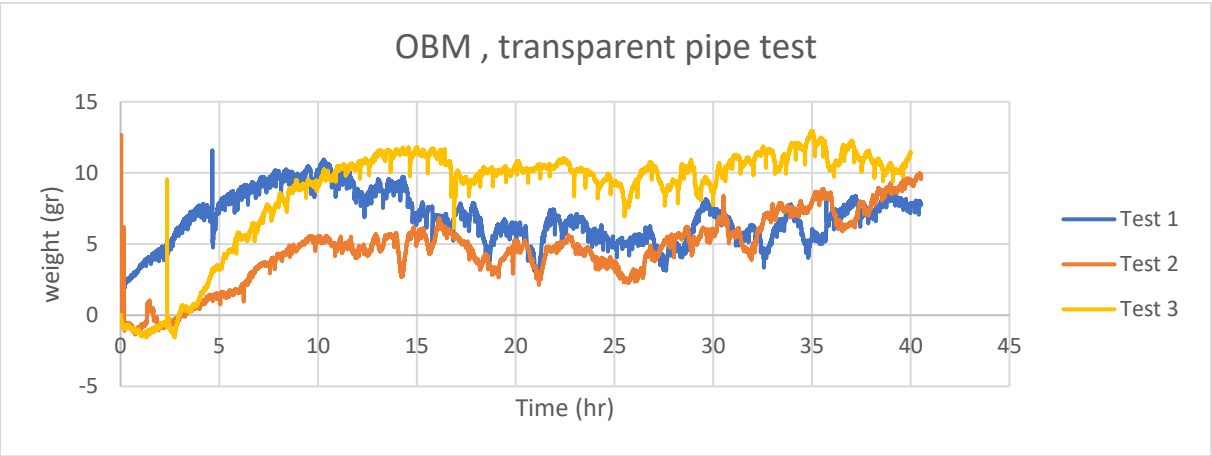

Figure 4- 26: Transparent pipe test results for the oil-based method

Figure 4.27 demonstrates the regression for different direct measurement test results in oil-based mud samples. It shows the trends and curve fitting for presenting adequate correlation to analysis the fluid behavior. Curve fitting specified the power model to obtain the best fit with highest R-square(0.6785) as it is presented by a correlation in the following :

$$Y = 0.8129\ x^{0.5967} \qquad \text{Eq 20}$$

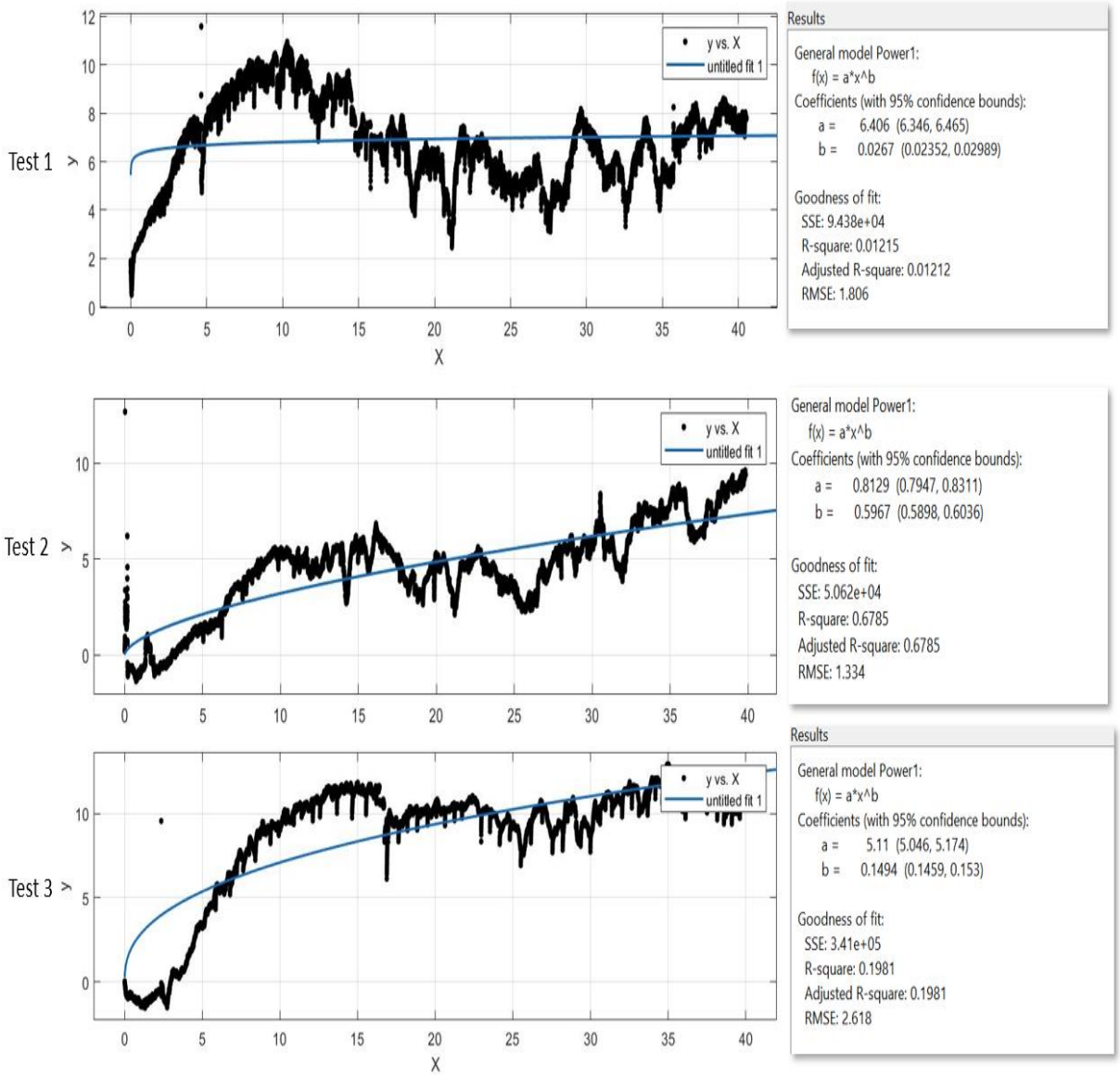

Figure 4- 27: Regression of transparent pipe test results for oil-based mud

Figure 4.28 shows the result from MPro experiment performed on OBM. The transit time had a rapid decrease at the first minutes of the test. Then the curve got constant for approximately 5 hours and started to decrease slowly until it reached 38.15 microsec/in. After 10 hours, the transit time increased gradually and peaked at 38.23 microsec/in and decreased smoothly to stabilize at the end of the test.

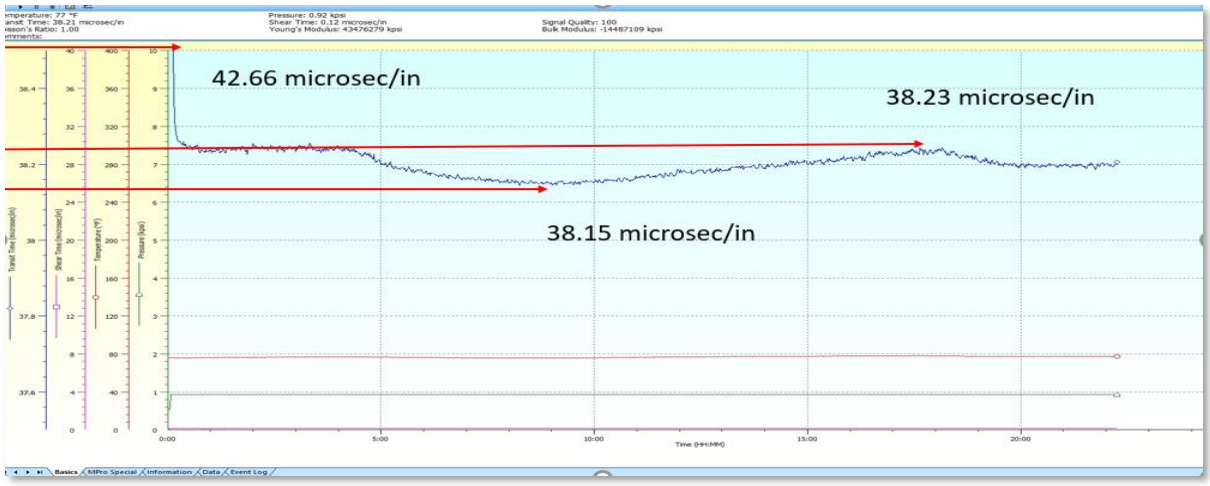

Figure 4- 28: MPro result for oil-based mud

Figure 4.29 compares the transit time trend with settled barite weight over time. A steep slope in decreasing the transit time is noticeable while sedimentation rate is high at the first phase of the test, and then they settled to have a smooth trend.

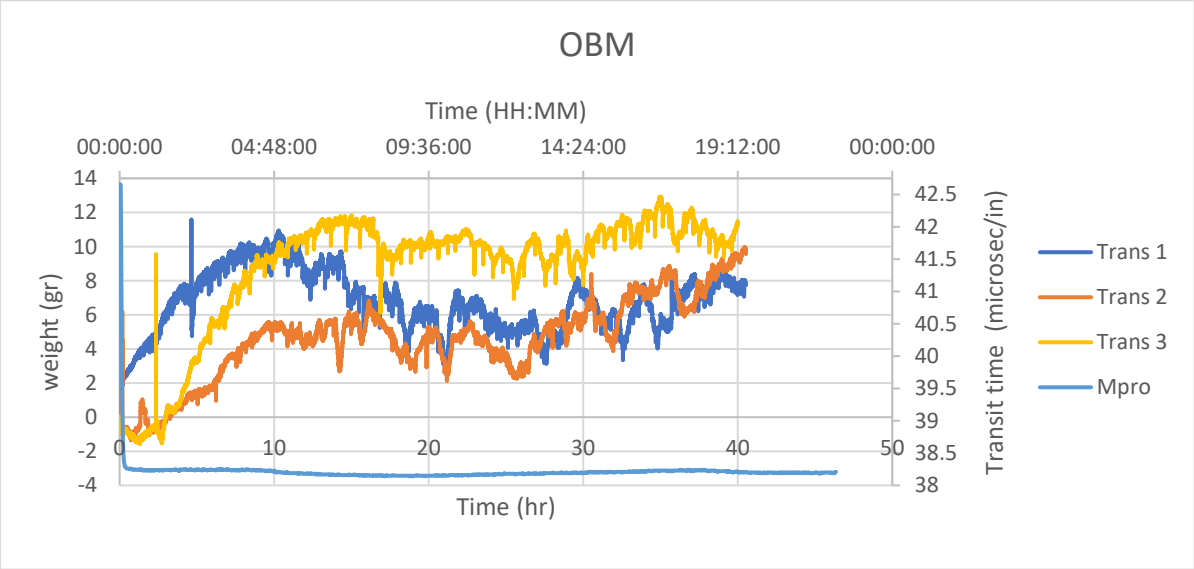

Figure 4- 29: MPro and transparent pipe test result comparison for oil-based mud

5. Conclusion

The following conclusions can be withdrawn as result of this project :

- In direct measurement for reference samples, XG content has an effect on the sag severity. With increasing the XG value, the sedimentation rate decreases. XG did not give any yield stress to suspend the particles. In other words, it only increased the viscosity of the carrier fluid.
- In direct measurement for real samples, sag potential in WBM is more than OBM since there is a higher sedimentation rate, and barite settled weight can reach a higher value. This could be due to the lack of gel-structure producing chemical such as bentonite.

- Within indirect measurement, transit time decreases over time due to the barite particle settling. After sedimentation, where there are fewer suspended particles, it takes less time to reach from transducer to receiver so that the propagated signals travel faster through media due to the less vibration.

- Hot rolling in WBM samples causes viscosity reduction so that the samples are less viscous after hot rolling.

- OBM samples get more viscosity after hot rolling. Yield stress has the same behavior and increases due to the hot rolling.

- Based on direct measurement results, empirical correlations have been obtained for reference samples, water-based mud, and oil-based mud to analyze the fluid behavior in barite settling. As further work, the appropriate parameters can be found to convert the empirical models to theoretical models.

Unsolved question

since the xanthan gum does not give substantial yield stress to the fluid, it is impossible to calculate the gel strength needed to prevent barite sag. Barite particle diameter criteria for settling can be calculated by yield stress, and then the whole weight of barite, which has the potential to settle, will be evaluated. Low shear rate viscosity is just given to the fluid due to the xanthan gum, and It is suggested to add other material such as bentonite for crossling the xanthan gum to develop the yield stress.

References

Arrow, B. (2015). *INSTRUCTION MANUAL MODEL 6265 Mechanical Properties Analyzer (MPRO ®)* (Issue November).

Bamberger, J. A., & Greenwood, M. S. (2004). Using ultrasonic attenuation to monitor slurry mixing in real time. *Ultrasonics*, *42*(1–9), 145–148. https://doi.org/10.1016/j.ultras.2004.02.016

Basfar, S., Salaheldin Elkatatny, A. A.-M., & Sheri, D. Al. (2020). *Prevention of Barite Sagging for Invert Emulsion Drilling Fluid While Drilling*. 1–11.

Batchelor, C. K., & Batchelor, G. K. (2000). *An introduction to fluid dynamics*. Cambridge university press.

Batchelor, G. K., & Wen, C. S. (1982). Sedimentation in a dilute polydisperse system of interacting spheres. Part 2. Numerical results. *Journal of Fluid Mechanics*, *124*, 495–528. https://doi.org/10.1017/S0022112082002602

Bern, P. A., Oort, E. Van, Neusstadt, B., Ebeltoft, H., Zurdo, C., & Zamora, M. (1998). *P.A. Bern, BP Exploration; E. van Oort and B. Neusstadt, Shell; H. Ebeltoft, Statoil; C. Zurdo, Elf; M. Zamora and K.Slater, M-1*.

Bern, P. A., Zamora, M., Hemphill, A. T., Marshall, D., Omland, T. H., & Morton, E. K. (2010). Field Monitoring of Weight-Material Sag. *The 2010 AADE Fluids Conference and Exhibition*.

Dye, W, Mullen, G., Gusler, W., Hughes, B., & Fluids, D. (n.d.). *IADC / SPE 98167 Field-Proven Technology To Manage Dynamic Barite Sag*.

Dye, William, Hemphill, T., Gusler, W., & Mullen, G. (1999). Correlation of ultra-low shear rate viscosity and dynamic barite sag in invert-emulsion drilling fluids. *Proceedings - SPE Annual Technical Conference and Exhibition, DELTA*, 543–553. https://doi.org/10.2118/56636-ms

Fard, A., Omland, T. H., & Saasen, A. (2007). Shale Shaker's Effect on Drilling Fluids Rheological Properties. *The Nordic Rheology Society*, *15*, 2–5.

Fjogstad, A., Saasen, A., Hagen, R., Tanche-Larsen, P. B., Ree, R., Melgren, H., Rostad, E., & Hoset, H. (2000). Field trial of alternative weight material with improved occupational hygiene and environmental performance. *International Conference on Health, Safety and Environment in Oil and Gas Exploration and Production*. https://doi.org/10.2523/61042-ms

Haghighi, E. B. (2015). *Single Phase Convective Heat Transfer with Nanofluids : An*

Experimental Approach " Doctoral Thesis. 1–116.

Hanson, P. M., Trigg, T. K., Rachal, G., & Zamora, M. (1990). Investigation of barite “sag” in weighted drilling fluids in highly deviated wells. *Proceedings - SPE Annual Technical Conference and Exhibition, Delta*, 223–230. https://doi.org/10.2523/20423-ms

Hashemian, Y., Miska, S., Yu, M., Ozbayoglu, E., Takach, N., & McLaury, B. (2014). Experimental study and modelling of barite sag in annular flow. *Journal of Canadian Petroleum Technology*, *53*(6), 365–373. https://doi.org/10.2118/173189-pa

Jamison, D. E., & Murphy Jr, R. J. (2003). *Apparatus and method for analyzing well fluid sag*. Google Patents.

Katzbauer, B. (1998). Polymer Degradarion and Smbilit,y 59 (1998) 8 I ~84 $~:t. *Polymer Degradation and Stability*, *59*(97), 81–84.

Khalifeh, M., & Saasen, A. (2020). *Introduction to Permanent Plug and Abandonment of Wells*.

Labastie, A. (2011). En Route: Letter from Russia. *Journal of Petroleum Technology*, *63*(02), 12–14. https://doi.org/10.2118/0211-0012-JPT

Maxey, J., Nguyen, T., Miska, S., & Yu, M. (2009). *Combined Effects Of Eccentricity And Pipe Rotation On Dynamic Barite Sag – Analysis The Different Impacts Of Pipe Rotation In A Flow Loop & Rotation In A Modified Rotational Viscom ... PIPE ROTATION ON DYNAMIC BARITE SAG – ROTATION IN A FLOW LOOP & ROTATI*. *April*.

Mjølhus, S. (2011). *Particle sedimentation detection using an ultrasonic cement analyser*. Norwegian University of Science and Technology.

Morita, I., Black, A. D., & Fuh, G. F. (1990). Theory of lost circulation pressure. *Proceedings - SPE Annual Technical Conference and Exhibition, Delta*, 43–58. https://doi.org/10.2523/20409-ms

NASA. (n.d.). *Shape Effects on Drag*. https://wright.nasa.gov/airplane/shaped.html

Omland, T. H., Hodne, H., Saasen, A., Mjølhus, S., & Amundsen, P. A. (2013). Drilling fluid weight material sedimentation - Sedimentation of suspensions. *Petroleum Science and Technology*, *31*(18), 1908–1915. https://doi.org/10.1080/10916466.2010.489085

Omland, T. H., Saasen, A., Taugbøl, K., Dahl, B., Jørgensen, T., Reinholt, F., Scholz, N., Ekrene, S., Villard, E., Amundsen, P. A., Amundsen, H. E. F., Fries, M., & Steele, A. (2007). Improved drilling-process control through continuous particle and cuttings monitoring. *Society of Petroleum Engineers - Digital Energy Conference and Exhibition*

2007, 250–256. https://doi.org/10.2523/107547-ms

Omland, Tor H, Øvsthus, J., Svanes, K., Saasen, A., & Jacob, H. (2004). *Weighting Material Sag*. *12*, 115–122.

Omland, Tor H, Saasen, A., & Amund, P. (2007). *Detection Techniques Determining Weighting Material Sag in Drilling Fluid and Relationship to Rheology*. *15*.

Omland, Tor Henry. (2009). *Particle Settling in non-Newtonian Drilling Fluids*. http://brage.bibsys.no/xmlui/bitstream/id/179394/Omland,

Rismanto, R., & Zwaag, C. Van Der. (2007). Explorative Study of NMR Drilling Fluids Measurement. *Rheology*, *15*.

Saasen, A., Liu, D., & Marken, C. D. (1995). *Prediction of Barite Sag Potential of Drilling Fluids From Rheological Measurements* . https://doi.org/10.2118/29410-MS

Schaflinger, U. (1985). Experiments on sedimentation beneath downward-facing inclined walls. *International Journal of Multiphase Flow*, *11*(2), 189–199. https://doi.org/10.1016/0301-9322(85)90045-X

Stokes, G. G. (1901). *MATHEMATICAL and PHYSICAL PAPERS vol III*.

Taugbøl, K., Svanes, G., Svanes, K., Omland, T. H., Alteras, E., & Mathisen, A. M. (2005). Investigation of flow-back properties of various drilling and completion fluids through production screens. *SPE - European Formation Damage Conference, Proceedings, EFDC*, 149–157. https://doi.org/10.2523/94558-ms

van der Zwaag, C. H., Stallmach, F., Basan, P. B., Hanssen, J. E., Soergaard, E., & Toennessen, R. (1997). New methodology to investigate formation damage using non-destructive analytical tools. In *SPE - European Formation Damage Control Conference, Proceedings* (pp. 173–185). https://doi.org/10.2523/38161-ms

Vrålstad, T., Saasen, A., Fjær, E., Øia, T., Ytrehus, J. D., & Khalifeh, M. (2019). Plug & abandonment of offshore wells: Ensuring long-term well integrity and cost-efficiency. *Journal of Petroleum Science and Engineering*, *173*(September 2018), 478–491. https://doi.org/10.1016/j.petrol.2018.10.049

Walker, D. M. (1966). An approximate theory for pressures and arching in hoppers. *Chemical Engineering Science*, *21*(11), 975–997.

Zamora, M. (2009). Mechanisms, measurement and mitigation of barite sag. *Offshore Mediterranean Conference and Exhibition 2009, OMC 2009*, 1–14.

Zamora, M., Bell, R., & Swaco, M. (2004). *Improved Wellsite Test for Monitoring Barite Sag. Paper AADE-04DF-HO-19 presented at the AADE 2004 Drilling Fluids Conference, Houston, Texas, USA, April 6-7*.